Multisatellite observations of a giant pulsation event

Kazue Takahashi,[1] Karl-Heinz Glassmeier,[2,3] Vassilis Angelopoulos,[4] John Bonnell,[5] Yukitoshi Nishimura,[6] Howard J. Singer,[7] and Christopher T. Russell[4]

Received 27 June 2011; revised 17 August 2011; accepted 8 September 2011; published 30 November 2011.

[1] Giant pulsations (Pgs; frequency ~10 mHz) were detected with ground magnetometers on the North American continent on 19 October 2008, when the GOES-10, -11, -12, and -13 geostationary satellites and the THEMIS-A probe were magnetically connected to the region of the ground pulsation activity. This unique configuration allowed us to determine the properties of magnetospheric ultra-low-frequency (ULF) waves that caused the Pgs on the ground. All spacecraft detected monochromatic ULF waves at ~10 mHz, and the coherence between the Pg at the Gillam ground station and the ULF wave at THEMIS-A was high when the magnetic field foot point of the spacecraft came close to the ground station. The ULF waves observed by the five spacecraft had perturbations in the radial and compressional components of the magnetic field and in the azimuthal component of the electric field, which are attributed to poloidal mode standing Alfvén waves. The poloidal waves were accompanied by multiharmonic toroidal waves, and from the frequency relationship among these, it is concluded that the ~10 mHz oscillations correspond to the fundamental (odd, or symmetric) mode. The standing wave mode also explains the amplitude variation with latitude and the phase delay between the magnetic and electric fields. Numerical models of poloidal waves incorporating finite height integrated ionospheric conductivity indicate that the fundamental mode interpretation is valid even when the damping of the standing waves is strong. Our observations are the most comprehensive to date in terms of spacecraft data, and we believe that theoretical work on the Pg generation mechanism should focus on mechanisms specific to odd mode standing waves, such as drift resonance of ring current ions.

Citation: Takahashi, K., K.-H. Glassmeier, V. Angelopoulos, J. Bonnell, Y. Nishimura, H. J. Singer, and C. T. Russell (2011), Multisatellite observations of a giant pulsation event, *J. Geophys. Res.*, *116*, A11223, doi:10.1029/2011JA016955.

1. Introduction

1.1. Historical Background

[2] Giant pulsations (Pgs) are a special type of ultra-low-frequency (ULF) waves that have been known about for more than a century since being first reported by *Birkeland* [1901]. This long history can be attributed to the fact that a Pg stands out even in magnetic field records from analog instruments. It is easy to see this point in the Pg event shown in Figure 1, which is the subject of the present paper. Leaving the details to later sections, a casual glance of the unfiltered ground magnetic field records (Figure 1e) tells us of the presence of highly regular oscillations (period ~100 s), which are localized to $L \sim 6$ and exhibit a strong east-west (Y) component. Here, L is the magnetic field shell parameter defined as $L = \cos^{-2}(\lambda_{CGM})$ in terms of the corrected geomagnetic (CGM) latitude λ_{CGM}. These characteristics distinguish Pgs from more commonly observed ULF waves in the Pc4 band (45–150 s period), which exhibit more irregular waveforms, stronger north-south perturbations, and a wider latitudinal span [e.g., *Samson and Rostoker*, 1972]. Statistical studies of ground magnetic field data have revealed additional intriguing characteristics of Pgs, including localization in the dawn sector, strong seasonal dependence with an activity peak at the equinox, and almost exclusive occurrence within a few years of the solar minimum [*Brekke et al.*, 1987]. Other important Pg characteristics known from ground-based observations are westward phase propagation and an azimuthal wave number in the range of 16–35 [*Rostoker et al.*, 1979; *Glassmeier*, 1980; *Hillebrand et al.*, 1982; *Poulter et al.*, 1983]. Despite these distinctive observable features of Pgs, the generation mechanism of the pulsations remains

[1]The Johns Hopkins University Applied Physics Laboratory, Laurel, Maryland, USA.
[2]Institute for Geophysics and Extraterrestrial Physics, Technical University of Braunschweig, Braunschweig, Germany.
[3]Max Planck Institute for Solar System Research, Katlenburg-Lindau, Germany.
[4]Institute of Geophysics and Planetary Physics and Department of Earth and Space Sciences, University of California, Los Angeles, California, USA.
[5]Space Sciences Laboratory, University of California, Berkeley, California, USA.
[6]Department of Atmospheric and Oceanic Sciences, University of California, Los Angeles, California, USA.
[7]NOAA Space Weather Prediction Center, Boulder, Colorado, USA.

0148-0227/11/2011JA016955

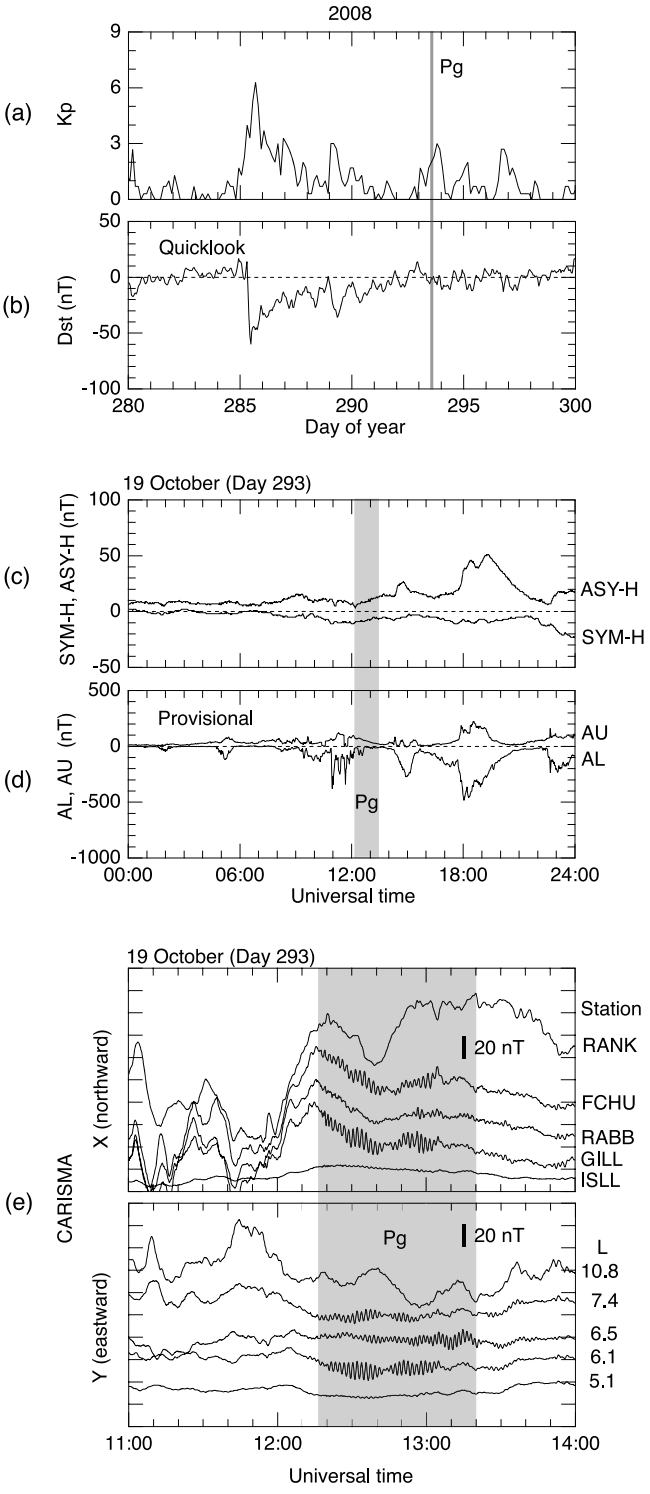

Figure 1. Geomagnetic activity indices and ground magnetic field records for the Pg event on 19 October (day 293) 2008. Shading indicates the time interval of ground Pg activity. (a) Three-hour Kp index. (b) Quicklook Dst index. (c) SYM-H and ASY-H indices. (d) Provisional AL and AU indices. (e) Magnetic field *X* (geographic north) and *Y* (geographic east) components at selected CARISMA sites. The station code and the magnetic field *L* parameter are shown on the right.

a mystery, although most researchers agree that Pgs originate from eigenmode oscillations of geomagnetic field lines (standing Alfvén waves) [e.g., *Veldkamp*, 1960] with a strong poloidal component (radial field line displacement) [e.g., *Chisham et al.*, 1992] that are excited by an energy source located within the magnetosphere [e.g., *Green*, 1979]. The strong *Y* component on the ground is attributed to the ionospheric 90 degree rotation of the major axis of polarization [*Hughes and Southwood*, 1976].

1.2. Standing Wave Mode and Excitation Mechanism

[3] A major Pg controversy concerns the standing wave harmonic mode: Is it odd or even? In the elastic string model of standing waves excited on Earth's magnetic field lines [e.g., *Sugiura and Wilson*, 1964], the lowest-order odd mode is the fundamental mode with its field line displacement pattern symmetric about the magnetic equator. The lowest-order even (antisymmetric) mode is the second harmonic. The third or higher harmonic is a mathematical possibility [e.g., *Cummings et al.*, 1969], but the Pg period of approximately 100 s means that we can exclude this possibility on the basis of the statistical distribution of the fundamental field line resonance frequency at $L \sim 7$ [*Chisham and Orr*, 1991; *Takahashi et al.*, 2010]. Note that following previous studies we will refer to the standing wave mode using the following sets of terms and that within each set the terms are used interchangeably. One set consists of "odd mode," "fundamental mode," and "symmetric mode," and the other set consists of "even mode," "second harmonic mode," and "antisymmetric mode."

[4] The standing wave mode constrains the possible types of ULF instability in the inner magnetosphere [*Southwood*, 1976; *Chen and Hasegawa*, 1991; *Cheng et al.*, 1994]. Consider for now excitation of standing Alfvén waves through resonance involving the drift and bounce motion of ring current ions [*Southwood*, 1976]. On the one hand, an inward gradient of ion phase space density at ring current energy can destabilize westward propagating odd mode waves through drift resonance $\omega - m\omega_d = 0$, where ω is the wave frequency, ω_d is the bounce averaged drift frequency, and m is the azimuthal wave number defined positive (negative) for eastward (westward) propagation. An important point noted by *Southwood* [1976] is that the gradient must be steeper than that associated with injection of hot plasma with the first two adiabatic invariants conserved. Consequently, Southwood considered that the ring current is marginally stable to the instability involving the drift resonance. Nonetheless, drift resonance has been proposed for Pgs by *Takahashi et al.* [1992] and *Thompson and Kivelson* [2001]. Whether a sufficiently steep gradient is formed remains to be seen.

[5] On the other hand, ion bump-on-the-tail energy distribution can destabilize even mode waves through drift bounce resonance $\omega - m\omega_d = \omega_b$, where ω_b is the bounce frequency. Because a quasi-steady background electric field makes the particle drift paths energy dependent, a bump-on-the-tail energy distribution is quite commonly formed in the ring current region if ions are injected from a nightside source. Simultaneous occurrence of a monochromatic second-harmonic standing Alfvén wave and a bump-on-the-tail ion distribution has been reported in space, in support of the drift-bounce resonance mechanism [*Hughes et al.*,

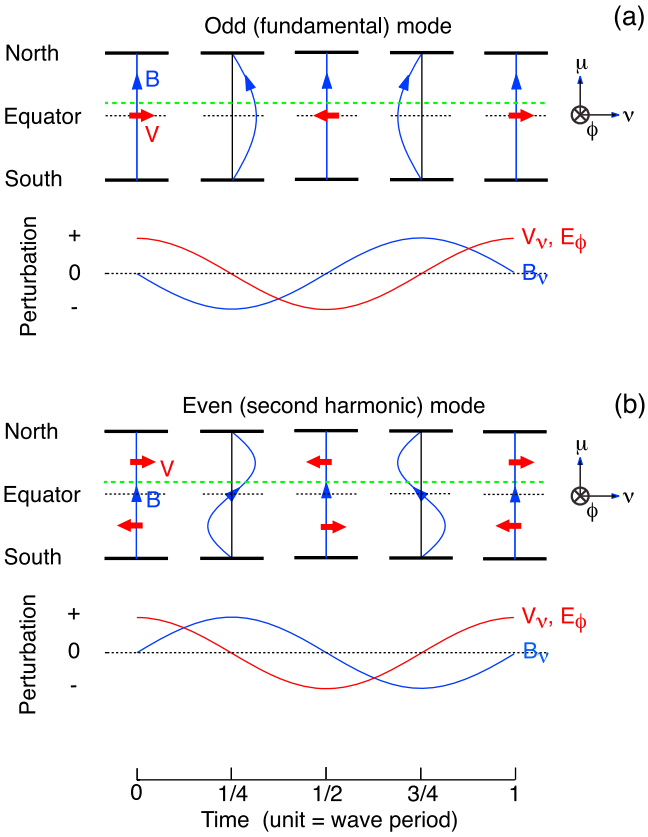

Figure 2. (a) The upper part shows snapshots of the field line pattern (blue curve with arrowhead) and plasma bulk velocity at the equator (red arrow) for an odd (fundamental or symmetric) mode field line oscillation in the magnetic meridian plane. The lower part shows the corresponding time series plots of the azimuthal (eastward) component of the electric field E_ϕ and the radial (outward) components of the velocity V_ν and magnetic field B_ν, measured at a fixed point in space slightly north of the magnetic equator (the green dashed line). (b) Same as Figure 2a except for an even (second harmonic or antisymmetric) mode oscillation.

1978]. This led many authors to argue that second-harmonic waves generated by this mechanism are the source of Pgs observed on the ground [*Poulter et al.*, 1983; *Chisham et al.*, 1990; *Chisham and Orr*, 1991; *Chisham et al.*, 1992; *Chisham*, 1996; *Chisham et al.*, 1997; *Wright et al.*, 2001; *Baddeley et al.*, 2002; *Baddeley et al.*, 2005a; *Wilson et al.*, 2006]. Note, however, evidence for one-to-one correspondence between a second-harmonic wave in space and a ground Pg is sparse [*Takahashi et al.*, 1992].

1.3. Need for Spacecraft Observations

[6] Observations on the ground produced contradicting results regarding the standing wave mode of Pgs. An early study using ground magnetometers placed at magnetically conjugate stations found an event showing the phase lag of even mode waves [*Annexstad and Wilson*, 1968]. However, other similar studies by *Green* [1979] and *Tonegawa and Sato* [1987] favored odd mode waves. Some authors inferred the harmonic mode from the statistical distribution of the Pg frequency. *Green* [1985] concluded that Pgs observed within the plasmasphere were odd mode (fundamental) waves. On the contrary, *Chisham and Orr* [1991] statistically analyzed the frequency of 34 Pgs and favored even mode (second harmonic) waves.

[7] Use of satellite data is essential for unambiguous mode identification because theoretically predicted properties of standing Alfvén waves can be directly observed in the magnetosphere. For qualitative understanding of how this works, Figure 2 shows the time sequence of the field line pattern and associated physical quantities over a wave period, using stretched field line geometry for the sake of simplicity [*Cummings et al.*, 1978]. For an ambient magnetic field, mass distribution, and ionospheric conductivity that are symmetric about the magnetic equator, the equator is the location of the nodes or antinodes of the standing waves. For odd mode waves, which include the fundamental mode, the equator is the location of a node of the transverse component of the magnetic field $\mathbf{B}_\perp$; the equator is also the location of an antinode of the field line displacement $\xi_\perp$, the transverse plasma bulk velocity $\mathbf{V}_\perp$, and the transverse electric field $\mathbf{E}_\perp$ ($=-\mathbf{V}_\perp \times \mathbf{B}_0$). Here we use boldface **B**, **E**, and **V** as short notation for the magnetic field, electric field, and plasma bulk velocity. For even mode waves, which include the second harmonic, the equatorial node and antinode are flipped for each physical quantity. Note that because we are interested in the poloidal mode, we are showing only the components relevant to that mode: V_ν, B_ν, and E_ϕ. The compressional component of the magnetic field B_μ, which is coupled to the transverse components in the real magnetosphere, has the same symmetry as E_ϕ. Therefore, if a satellite is located at the magnetic equator, measurements of any of the above quantities provide useful information on the equatorial node or antinode.

[8] If simultaneous measurements of both **B** and **E** (or **V**) are possible, we can use the phase and amplitude relation between them to determine the harmonic mode even when the satellite is located off the equator. For example, assume that we can measure E_ϕ and B_ν at the latitude indicated by a green dashed line in Figure 2. In this case we have an odd (even) mode wave if B_ν leads (lags) E_ϕ by 90°. In section 5 we show numerical models of standing waves using a dipole magnetic field and realistic ionospheric boundary conditions, but the wave properties near the magnetic equator are essentially the same as those illustrated in Figure 2. Finally, if we can measure the plasma density, it gives a strong constraint on the frequency of the standing wave, hence the harmonic mode.

[9] Previous satellite studies examined the nodal structure of oscillations in **B** and/or **E** associated ground Pg events and found evidence for odd mode waves. Most of these studies were done at geostationary orbit and using only **B** field data [*Kokubun*, 1980; *Hillebrand et al.*, 1982; *Kokubun et al.*, 1989] with the exception of the GEOS-2 study, which included **E** field data [*Glassmeier et al.*, 1999]. The compressional Pc4 event at the ATS-1 geostationary satellite reported by *Barfield et al.* [1971] and *Lanzerotti and Tartaglia* [1972] was later related to Pgs by *Green* [1979]. In the only study that used a satellite on an elliptical orbit (AMPTE/CCE), only **B** field data were available [*Takahashi et al.*, 1992]. These studies reported that (1) quantities associated with poloidal (meridional) motion of field lines, E_ϕ,

Table 1. List of Ground Magnetometer Sites

Site	Site Code	Geographic Latitude (deg)	Geographic Longitude (deg)	CGM Latitude (deg)	CGM Longitude (deg)	L
			CARISMA			
Dawson City	DAWS	64.0	220.9	65.9	274.0	6.0
Fort Churchill	FCHU	58.8	265.9	68.4	333.6	7.4
Fort Simpson	FSIM	61.8	238.8	67.3	294.3	6.7
Gillam	GILL	56.4	265.4	66.1	333.1	6.1
Gull Lake	GULL	50.1	251.7	58.2	315.0	3.6
Island Lake	ISLL	53.9	265.3	63.7	333.4	5.1
Ministik Lake	MSTK	53.4	247.0	60.7	308.0	4.2
Pinawa	PINA	50.2	264.0	60.0	331.8	4.0
Rabbit Lake	RABB	58.2	256.3	66.9	319.2	6.5
Rankin Inlet	RANK	62.8	267.9	72.3	336.1	10.8
			THEMIS-GBO			
Inuvik	INUV	68.3	226.7	71.2	276.2	9.6
Kapuskasing	KAPU	49.4	277.6	59.6	352.0	3.9
Kuujjuarapik	KUUJ	55.3	282.3	65.0	359.4	6.0
Flin Flon	TPAS	54.8	258.1	63.9	322.6	5.2
White Horse	WHIT	60.7	224.9	63.4	279.9	5.0

and B_v, were stronger than those associated with toroidal (azimuthal) motion of field lines, E_v and B_ϕ; (2) near the equator (magnetic latitude (MLAT) <5°), appreciable amplitude was detected in E_ϕ and B_μ, but not in B_v; and (3) away from the magnetic equator (MLAT ~ 10°), the B_v amplitude became appreciable. These features are all consistent with odd mode waves with a strong poloidal component. The AMPTE/CCE study [*Takahashi et al.*, 1992] included a systematic search for even mode waves in space that produce ground Pg signals, but the search produced a null result.

[10] To summarize previous studies, satellite observations overwhelmingly favor odd mode waves for Pgs, but there exists a school of thought for even mode waves based on observations of Pgs on the ground and investigation of ion energy distribution in space. This means that conclusive observations of the wave mode are warranted to advance our understanding of the generation mechanism of Pgs.

1.4. Organization of the Present Work

[11] In this paper, we combine data from five satellites and numerous ground magnetometers to unambiguously determine the standing wave mode of the Pgs shown in Figure 1. We conclude that the Pgs are related to odd mode standing waves excited at the fundamental frequency, in agreement with previous satellite observations. We also present new information on the properties of the Pg event, including the variation of magnetic field polarization with distance from the magnetic equatorial plane, variation of the frequency with local time and radial distance, the radial localization relative to the plasmapause, the radial component of the Poynting flux, equatorial observation of non-sinusoidal waveform, and the relationship between the plasma density and the pulsation frequency. Finally, we provide an explanation to some previous studies that favored even mode waves based on the observed frequency of Pgs. We believe that information obtained in this study strongly suggests that it is now time to focus on odd mode waves when investigating the excitation mechanism of Pgs. Measurements of ring current particles that are likely related to generation of the pulsations were made from the THEMIS spacecraft, but analysis of the particle data is left for future studies.

[12] The remainder of the paper is organized as follows. Section 2 describes the experiments used to acquire data used in the study. Sections 3 and 4 describe ground and satellite data, respectively. Section 5 presents discussion, and section 6 concludes the study.

2. Experiments

[13] The primary sources of data used in this paper are the THEMIS-A probe, the GOES-10, -11, -12, and -13 geostationary satellites, and the CARISMA and THEMIS Ground Based Observatory (GBO) magnetometer arrays. The relevant experiments are an electric field instrument [*Bonnell et al.*, 2008] and a fluxgate magnetometer [*Auster et al.*, 2008] on THEMIS-A, fluxgate magnetometers on GOES [*Singer et al.*, 1996], and fluxgate magnetometers on the ground in the CARISMA [*Mann et al.*, 2008] and THEMIS-GBO [*Russell et al.*, 2008] arrays. The position parameters for the ground magnetometers are listed in Table 1, where the magnetic coordinates are obtained for year 2008 using the online utility provided by Virtual Ionosphere, Thermosphere, Mesosphere Observatory (VITMO) (http://omniweb.gsfc.nasa.gov/vitmo/cgm_vitmo.html). Fields data from these experiments were time averaged to 3 or 5 s resolution, and the vector data from the satellites were rotated into coordinates that are referenced to a model magnetic field (specifics are described below). When computing cross spectra of data from different sources, we resample data at common time stamps after liner interpolation.

[14] We would like to point out that although the THEMIS mission has the substorm triggering mechanism as the main target of its investigations, the mission turned out to be ideal for studying Pgs as well. The mission covers the minimum phase of solar activity, the most likely epoch for Pg occurrence. Moreover, the THEMIS-A, -D, and -E, probes, which had low apogee distances and were in synchronization with North American ground magnetometers, passed the $L \sim 6$ region in the dusk sector during the fall of 2008. These factors

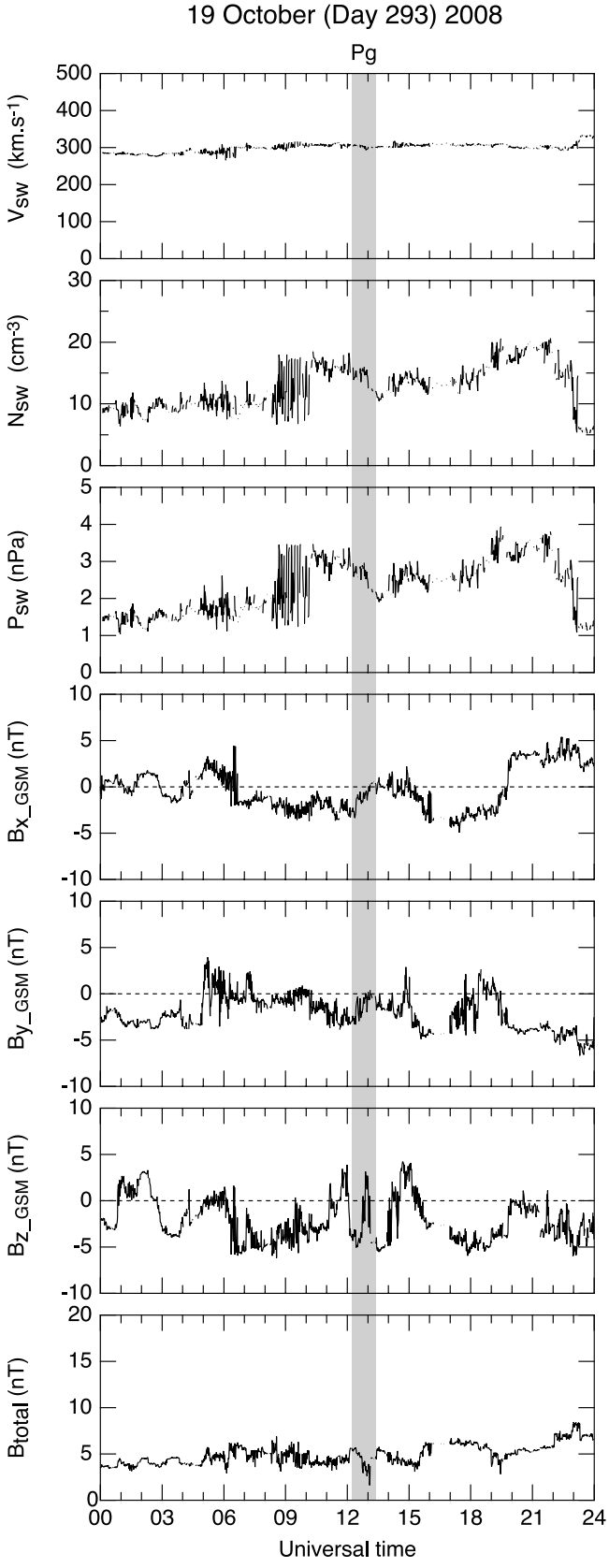

all maximize the probability of detecting Pgs [e.g., *Brekke et al.*, 1987].

3. Ground Data

3.1. Geomagnetic and Solar Wind Conditions

[15] The event shown in Figure 1 was identified by visual inspection of CARISMA magnetometer data acquired in the fall of 2008. There were other Pg events in that season, but this one was the best in terms of ground-THEMIS conjunction. As stated in the introduction, the time series plots of raw data (Figure 1e) are sufficient to demonstrate that the oscillations seen from 1215 to 1320 Universal Time (UT) (highlighted by shading) at GLLL, RABB, and FCHU can be classified as a Pg event in reference to previous reports on Pgs. The pulsation event occurred when Kp was modest (~2, Figure 1a) and Dst was close to zero (no geomagnetic storm, Figure 1b), but it was preceded by moderate auroral activity as inferred from the auroral electrojet indices (Figure 1d). The AL value reached −400 nT in the preceding 2 h.

[16] In relation to the geomagnetic indices shown in Figure 1, we show in Figure 3 the solar wind velocity, density, dynamic pressure, and the interplanetary magnetic field (IMF) vector in the GSM coordinates for 19 October 2008. The velocity was steady at a low value of ~300 km/s, but there was a density increase at ~0900 UT from ~10 cm^{-3} to ~15 cm^{-3} and the associated increase of the dynamic pressure from ~1.5 to ~3 nPa. The weak B_x and strong B_z components during the Pg event, highlighted by gray shading, means that the IMF cone angle was large and precludes the possibility that upstream ULF waves contributed to the Pg pulsation [*Troitskaya et al.*, 1971]. The magnetopause standoff distance given by the empirical formula of *Shue et al.* [1998] is approximately 11 R_E during the Pg event, which, combined with the low solar wind velocity, makes the magnetopause Kelvin-Helmholtz instability an unlikely source mechanism for the Pg event observed at $L \sim 6$. The auroral activity seen in Figure 1d is consistent with the interplanetary magnetic field, which was directed southward during much of the ~6 h period preceding the Pg event. We speculate that the auroral activity was related to injection of the ring current ions that contributed to the occurrence of the Pg event. However, because the ASY-H index (Figure 1c) did not rise in association with this activity, it appears that localized injection or formation of partial ring current was not very strong.

3.2. Latitude Dependence of Pulsation Properties

[17] To further demonstrate that our Pg event shared wave properties with previously reported Pg events, we show in Figure 4 magnetic field hodograms at 15 CARSIMA and THEMIS-GBO stations. In this figure the locations of the satellite foot points, calculated using the combined T89c

Figure 3. Solar wind bulk parameters, V_{SW} (velocity), N_{SW} (density), P_{SW} (dynamic pressure), and the IMF in the GSM coordinates for 19 October 2008, provided by the NASA National Space Science Data Center as High Resolution OMNI data. The data have a time resolution of 1 min and have been time shifted to the bow shock nose. The shading indicates the period of ground Pg activity shown in Figure 1.

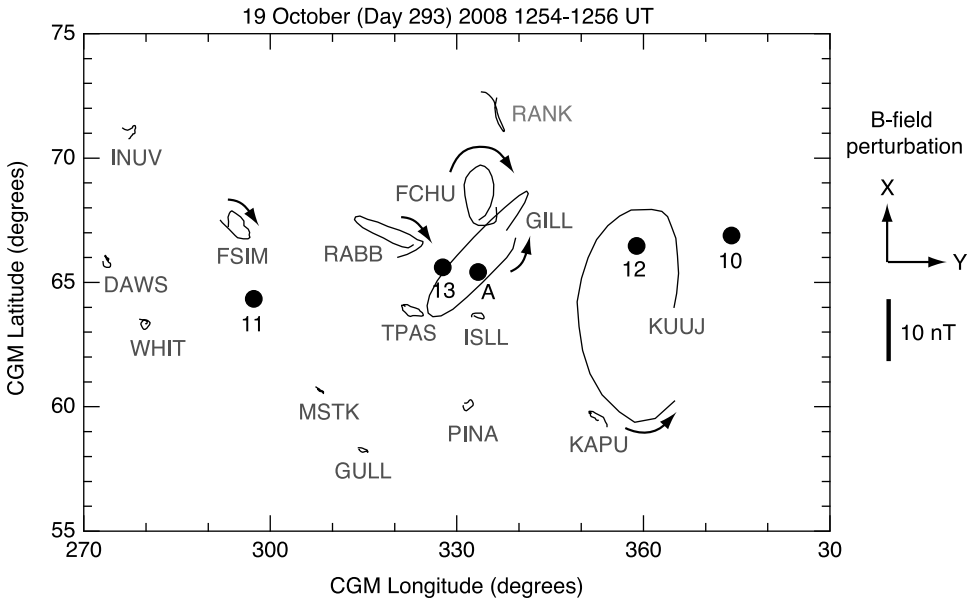

Figure 4. Composite of the map of satellite magnetic field foot points and magnetic field hodograms on the ground during a 2 min interval (1254–1256 UT) of the Pg event on 19 October 2008. The satellites are GOES-10 (10) through -13 (13) and THEMIS-A (A). The satellite foot points are based on the combined T89c and IGRF magnetic field model. The corrected CGM coordinates are used for the map, while the geographic X (north) and Y (east) coordinates are used for the hodograms. The hodograms are centered at the location of the magnetometers, with the amplitude scale given on the right. The sense of rotation of the field perturbation is shown at locations with large pulsation amplitude.

[*Tsyganenko*, 1989] and International Geomagnetic Reference Field (IGRF) models, are also shown in the CGM coordinates. Note that the CGM coordinates (latitude, longitude) of a point in space are computed by tracing the IGRF magnetic field line from that point to the dipole geomagnetic equator, then returning to the same altitude along the dipole field line and assigning the obtained dipole latitude and longitude as the CGM coordinates to the starting point (http://modelweb.gsfc.nasa.gov/models/cgm/cgmm_des.html). Figure 4 covers a 2 min window from 1254–1256 UT, corresponding to the center of Pg activity shown in Figure 1. The magnetic field time series was highpass filtered (low frequency cutoff at ~5 mHz) prior to generation of the hodograms. The largest amplitude was seen near the CGM latitude of 65°, indicating latitudinal localization of the pulsation. Looking at the hodograms along the ~330° CGM meridian, we find that the perturbation vector rotated counterclockwise at GILL (L = 6.1), oscillated almost linearly in the East-West direction at RABB (L = 6.5), and rotated clockwise at FCHU (L = 7.4). This latitudinal variation is qualitatively the same as those reported previously [*Glassmeier*, 1980; *Chisham et al.*, 1990], which leads us to believe that our Pg event is a typical one. The linear East-West polarization at RABB and change of the sense of rotation near this station implies that RABB was very near the latitudinal center of the Pg event. However, an accurate determination of the central latitude is difficult because the magnetometers are not very densely distributed in latitude. *Chisham et al.* [1997] statistically found that the Y-component amplitude of Pgs shows a full L width at half maximum value of ~1 (~2° in magnetic latitude), implying that we need a few more stations between GILL and FCHU to find the precise location of the peak amplitude.

3.3. Azimuthal Phase Variation

[18] Ground magnetometer data also provide information on the azimuthal phase variation of the pulsations. Figure 5 shows the waveform and spectral properties of the ground Y components at TPAS (CGM latitude = 63.9°, CGM longitude = 322.6°) and ISLL (63.7°, 333.4°) for 1230–1245 UT. These stations were chosen because they are essentially on the same magnetic latitude but are longitudinally separated with a distance comparable to the azimuthal wavelength of previously reported Pg events. Figure 5a shows that the stations, located some distance equatorward of the Pg amplitude peak, detected Pg signals with amplitude (~1 nT) much lower than that at the peak (~10 nT). Note that a quadratic function has been fitted to and subtracted from the original time series and that the detrended time series was used to generate the spectra, a procedure that was applied to all waveform and spectral analyses presented below.

[19] Although the amplitude was strongly dependent on latitude, we assume that the azimuthal wave number was not. The time series plots (Figure 5a) indicate that the pulsations at the two stations were very similar but were nearly in antiphase. This is confirmed in the nearly identical power spectra (Figure 5b) peaking at ~10 mHz, high coherence (Figure 5c), and the cross phase indicating that ISLL led TPAS by 163° (Figure 5d). Dividing the phase difference by the longitudinal separation of the stations 10.8°, we get $m = -15$ (westward propagation). Allowing for an additional 2π (360°) to the apparent phase difference, we get an alternative value of m = 18 (eastward propagation). Although we do not have additional data to remove the 2π uncertainty, the fact that we get $m = -15$ as a possible solution means that the event is

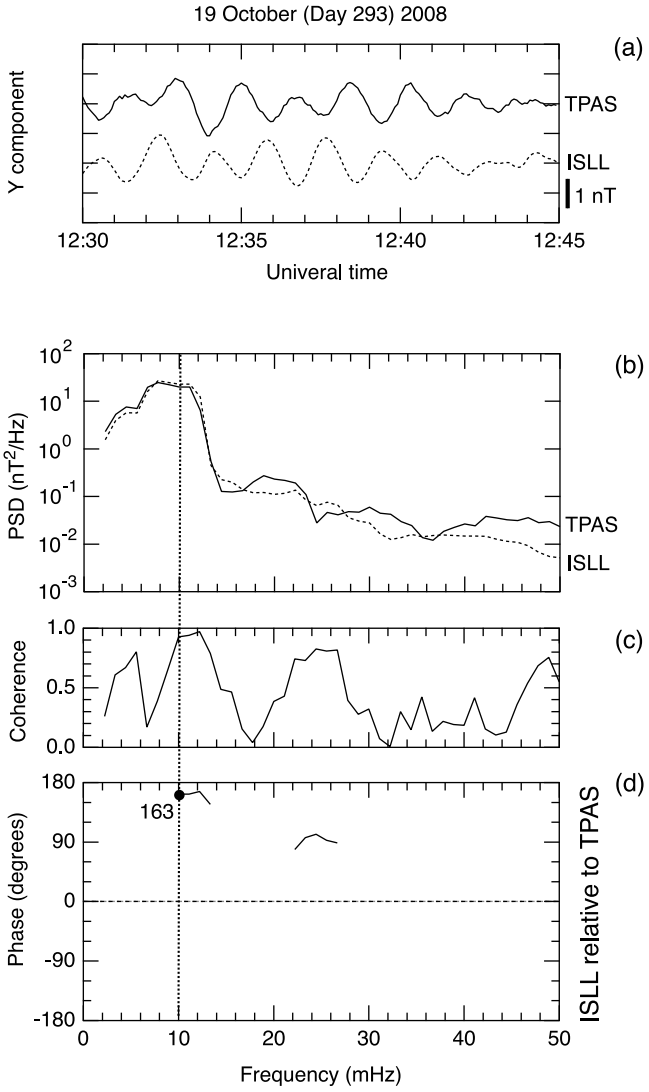

Figure 5. Waveform and spectral properties of the ground magnetic field *Y* (eastward) component at TPAS and ISLL. The spectral parameters were smoothed by five-point averaging. The vertical line at 10 mHz indicates the frequency of the Pg pulsation at GILL and FCHU. (a) Waveform. (b) PSD. (c) Coherence. (d) Cross phase, shown only if the coherence is higher than 0.7.

consistent with previously reported Pgs. For example, *Poulter et al.* [1983] obtained a comparable value $m \sim -17$ for a Pg event observed with the STARE radar. To summarize the ground observations, all observed properties of the pulsation event on 19 October (day of year 293) 2008, give us reason to believe that a typical Pg event occurred.

4. Spacecraft Data

4.1. Spacecraft Location

[20] What makes the Pg event very special is the fact there were multiple spacecraft in the equatorial region that was threaded by field lines connected to the ground Pg event. In Figure 4 we have included magnetic field line mapping of the satellites to the ground for the epoch of 1255 UT on 19 October 2008, when the pulsation amplitude at THEMIS-A peaked. The foot points approximately form a straight line that lies in the middle of the ground Pg activity. Moreover, THEMIS-A, which was the best-instrumented among the five satellites shown here, had its foot point very close to the CARISMA GILL station. Assuming that Pgs propagate from the magnetosphere to the ground along the background magnetic field line, we have an ideal ensemble of satellites and ground stations to study the magnetospheric wave mode of Pgs. Figure 6 shows the location of the five spacecraft for 1215–1315 UT in an *L* (radius) versus magnetic local time (MLT) polar map, where *L* and MLT are based on a centered dipole. The four GOES satellites were located in the dawn sector, and the THEMIS-A probe was near the dawn meridian, moving outward from $L = 5.6$ to $L = 6.9$. THEMIS-A was closest to GOES-13.

4.2. Plasma Density Radial Profile

[21] The elliptical orbit of THEMIS-A and the electric field experiment on the spacecraft allow us to estimate the radial profile of the electron number density and to determine the location of the plasmapause. It is of great interest to find the plasmapause location relative to the region of Pg pulsations, since there have been ground observations of Pg events at plasmaspheric latitudes [*Green*, 1985] and a suggestion that Pgs occur at the plasmapause [*Rostoker et al.*, 1979] or are excited in the presence of cold plasma [*Green*, 1979, 1985]. In previous satellite studies of Pgs, there was no information on the plasma density radial profile.

[22] Figure 7 compares the radial profiles of the electron density n_e and pulsation amplitude. The electron number density (Figure 7a) was derived from the spacecraft potential data [*Li et al.*, 2010] for the outbound leg of the THEMIS-A orbit that encountered the Pg event, 1030–1600 UT on 19 October 2008, plotted as a function of field line maximum distance R_{max} (normalized to earth radius, R_E). The R_{max} parameter was calculated using the T89c/IGRF model. The electron density has a factor of 2 uncertainty about the

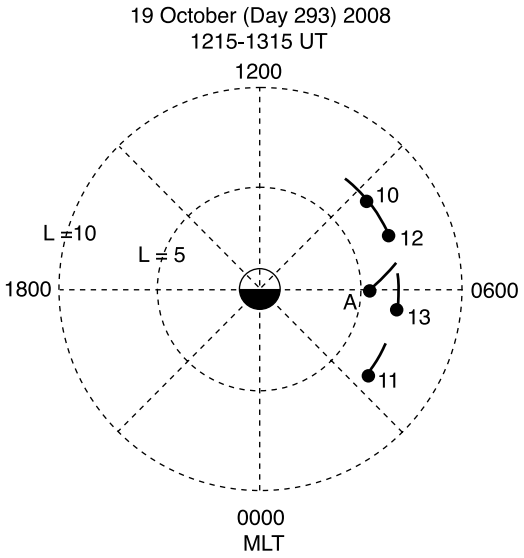

Figure 6. *L* versus MLT positions of the GOES-10 through -13 and THEMIS-A satellites for 1215–1315 UT on 19 October 2008. The heavy dots indicate the location at 1215 UT.

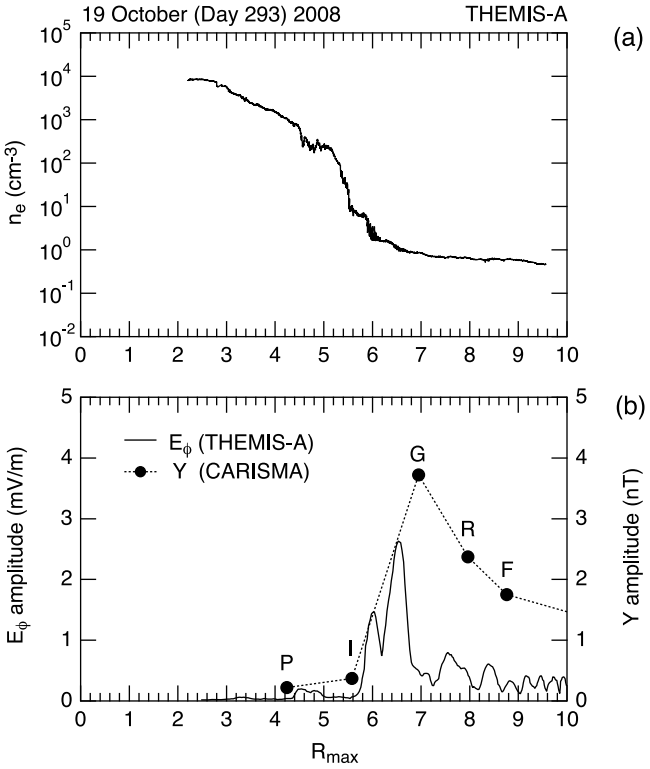

Figure 7. (a) Electron density n_e estimated from the spacecraft potential at THEMIS-A versus field line maximum distance R_{max}. The R_{max} values are based on the combined T89c for Kp = 2 and IGRF magnetic field model. The data cover 1030–1600 UT on 19 October 2008. (b) ULF wave amplitude in space and on the ground versus R_{max}. See text for the definition of the amplitude.

nominal value plotted, but it is accurate enough for detecting steep density gradients. On this particular orbit, a plasmapause gradient is seen from $R_{max} \sim 5$ ($n_e \sim 260$ cm^{-3}) to $R_{max} \sim 6$ (~2 cm^{-3}).

[23] Figure 7b shows the R_{max} dependence of the pulsation amplitude. The continuous line is the root mean square (rms) amplitude of the E_ϕ component at THEMIS-A, which represents the poloidal mode. The amplitude was obtained by first computing the power spectral density (PSD) of E_ϕ in a 10 min moving time window, integrating the PSD from 3 to 15 mHz, and taking the square root of the integrated power. The wide frequency band was chosen to capture the spatially varying fundamental field line frequency as the spacecraft moved radially (see Figure 12). The solid circles connected by a dotted line show the similarly defined RMS amplitude of the ground magnetic field Y components in the 5–15 mHz band at five CARISMA stations located near the 330° magnetic meridian. The ground amplitude was evaluated for the 1245–1305 UT segment. When mapping from the ground to the magnetic equator, the L parameter differs significantly from R_{max}, so the use of the latter is essential. For example, we have $L = 7.4$ and $R_{max} = 8.8$ for FCHU. Under the assumption that the plasmapause location did not vary much with UT or MLT, we can conclude that both the magnetospheric poloidal waves and the ground Pg pulsations had appreciable amplitude only outside of the outer edge of the plasmapause ($R_{max} \sim 6.0$), with an amplitude peak occurring at $R_{max} =$ 6.5 (THEMIS-A) or $R_{max} \sim 7.0$ (CARISMA). Because the ground magnetometers are relatively sparsely located, the actual ground peak location could be very close to the satellite estimate.

4.3. Dynamic Spectra

[24] Dynamic spectra of field components provide valuable information on the frequency and polarization of ULF waves. Figure 8 shows dynamic spectra of magnetic field data from GOES-10, -11, and -13, and CARISMA-GILL for a 5 h interval encompassing the Pg event detected on the ground. The three GOES spacecraft represent the full longitudinal span covered by the geostationary satellites, with GOES-10 farthest east, GOES-13 closest, and GOES-11 farthest west relative to THEMIS-A and GILL. At GOES, the magnetic field vectors are expressed in the local v-ϕ-μ coordinates where the coordinate axes $\mathbf{e}_v$ (transverse to the background magnetic field, positive outward), $\mathbf{e}_\phi$ (azimuthal, positive eastward), and $\mathbf{e}_\mu$ (magnetic field aligned) are defined in reference to the T89c/IGRF model magnetic field [*Tsyganenko*, 1989], which is a good approximation to the observed field in the magnetospheric region considered here.

[25] The spectrograms demonstrate a close connection between the ground Pg pulsations and ULF waves in space, which forms the basis of our conclusion that the spacecraft indeed detected the source ULF waves that produced the Pg signals on the ground. The Pg pulsation at GILL is seen as a strong narrowband spectral enhancement at 10 mHz in the Y (eastward) component occurring at ~1300 UT. Corresponding to this ground Pg signal, all GOES satellites detected similarly narrowband oscillations at or near 10 mHz. At each GOES satellite, either B_v or B_μ exhibited the highest intensity, which puts the pulsations in space into the compressional poloidal (rather than toroidal) mode in terms of magnetic field polarization. The relative spectral intensity of B_v and B_μ varies from one satellite to another. GOES-11, located at the lowest MLAT of 4.6°, detected highest power in B_μ. GOES-13, located at MLAT = 8.5°, detected comparable power in B_v and B_μ. GOES-10, located at the highest latitude MLAT = 9.9°, detected higher power in B_v.

[26] In addition to the 10 mHz poloidal wave, each GOES spacecraft detected signatures of multiharmonic toroidal waves. Toroidal waves are seen most clearly at GOES-10. This is because this spacecraft was at the highest magnetic latitude and the waves tend to be excited stronger at odd harmonics, which have a B_ϕ node at the equator [*Takahashi and McPherron*, 1982]. The second harmonic (labeled f_{T2}) and the third harmonic (labeled f_{T3}) are visible in this display format.

[27] Figure 9 shows a comparison of the **E** and **B** spectra (Figure 9a) at THEMIS-A and the Y spectra at GILL (Figure 9b, repeated from Figure 8) for the same 5 h interval. Figure 9 also demonstrates a close connection between ULF waves in space and Pgs on the ground. THEMIS-A was moving outward from $L = 3.4$ to $L = 9.6$ and encountered the Pg event at ~1300 UT, $L \sim 6.6$, MLAT ~ 4°, and MLT ~ 6.7 h (Figure 9a). The magnetic field signature of the Pg at THEMIS-A is quite similar to that at GOES-13 shown in Figure 8: a strong spectral peak appears in B_μ at ~10 mHz. The electric field spectra at THEMIS-A also show strong power at the same frequency in both the radial (E_v) and the azimuthal (E_ϕ) components, with E_ϕ being the stronger

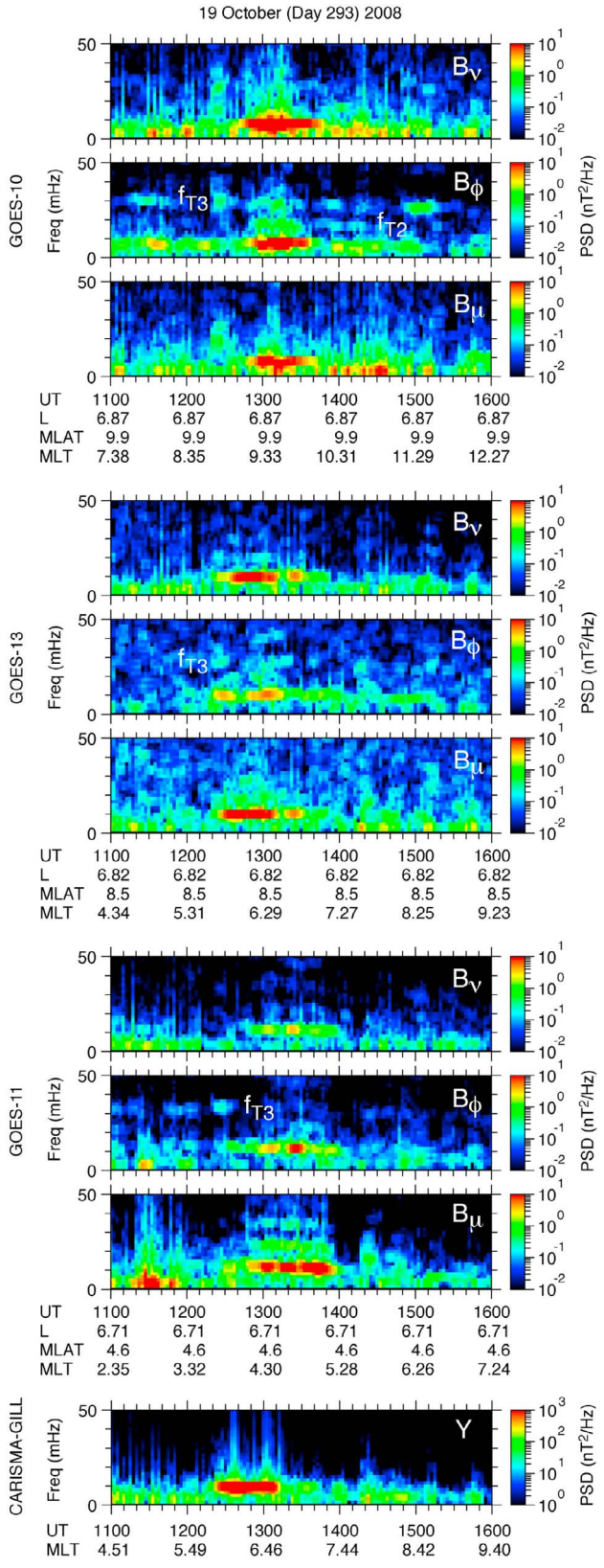

Figure 8. Dynamic spectra of magnetic field at the GOES satellites and a CARISMA station for a 5 h period including the Pg event on 19 October 2008. Magnetic coordinates L, MLAT (in degrees), and MLT (in hours), defined using a centered dipole, are shown for each GOES satellite.

between the two (better seen in the waveform plots of Figure 10). The coherence spectra shown at the bottom (Figure 9c) indicate that coherence is elevated at ~1300 UT at the Pg frequency of ~10 mHz, confirmation that there was a causal relationship between the poloidal wave in space and the Pg on the ground.

[28] We note that although the ground Pg ended abruptly at 1310 UT, narrowband pulsations continued at THEMIS-A until 1600 UT, the end of the time period shown. The amplitude and polarization of the pulsations varied, but the frequency was on a steady decreasing trend as the satellite moved outward, from 10 mHz at $L = 6.0$ to 5 mHz at $L = 9$. During that later part of this ULF wave activity, E_ν and E_ϕ exhibited comparable amplitude, unlike at ~1300 UT when E_ϕ was much stronger.

4.4. Waveform and Spectra

[29] Figure 10 presents further details of the spatial variation of ULF waves in space, focusing on the 20 min interval

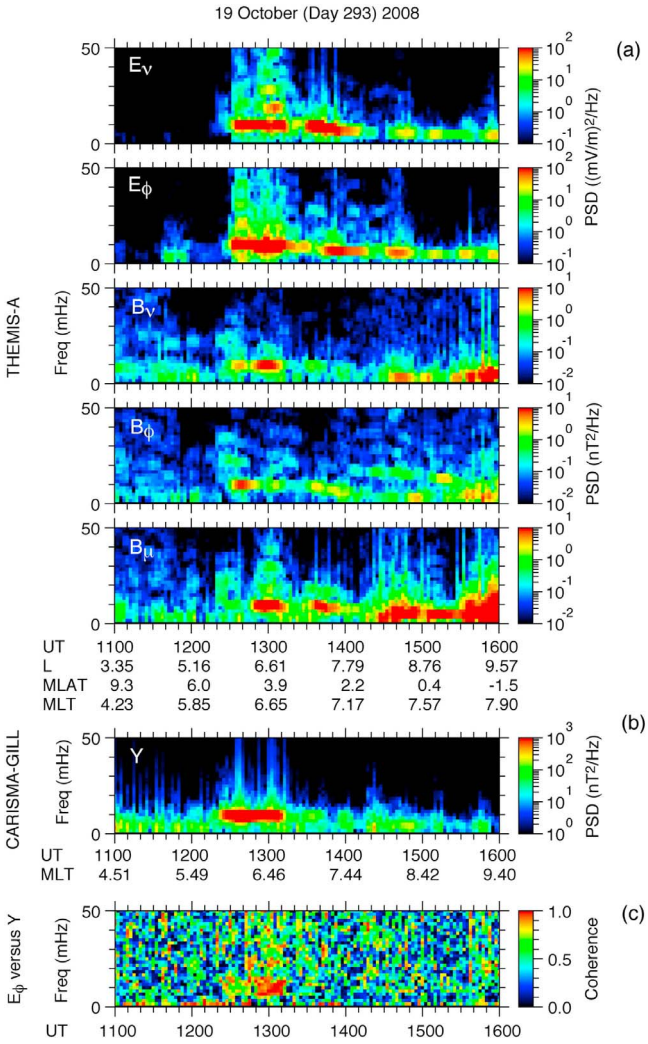

Figure 9. Dynamic display of spectral parameters for a 5 h period including the Pg event on 19 October 2008. (a) PSD of the electric and magnetic fields at THEMIS-A. (b) PSD of the ground Y (eastward) component at GILL. (c) Coherence between E_ϕ at THEMIS-A and Y at GILL.

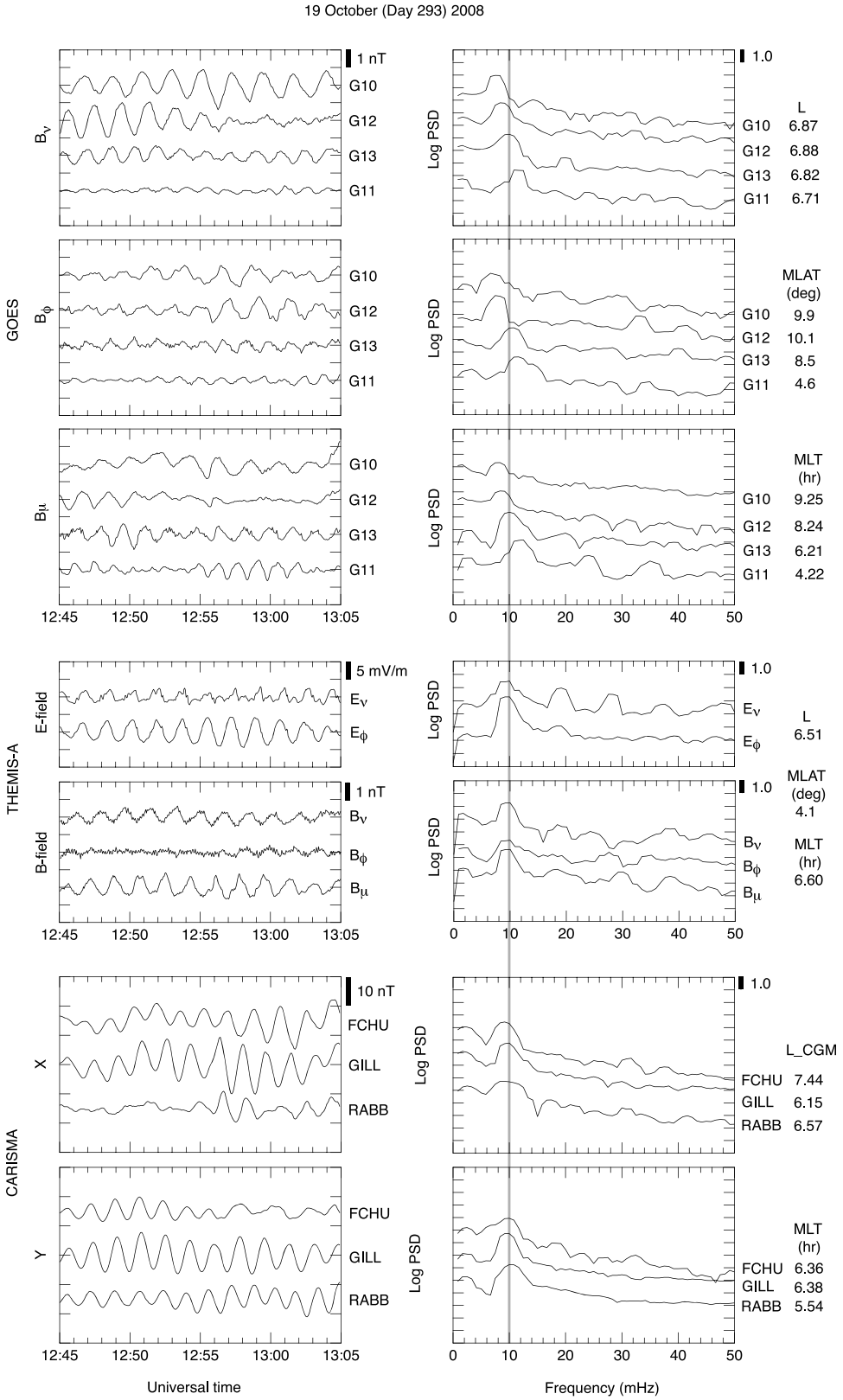

Figure 10. Waveform and spectra of satellite and ground data for 1245–1305 UT on 19 October 2008. The vertical line drawn over the spectra marks the frequency, 10 mHz, of the Pg observed on the ground at FCHU, GILL, and RABB. The magnetic coordinates, *L*, MLAT, and MLT of each observatory are shown on the right of the spectra.

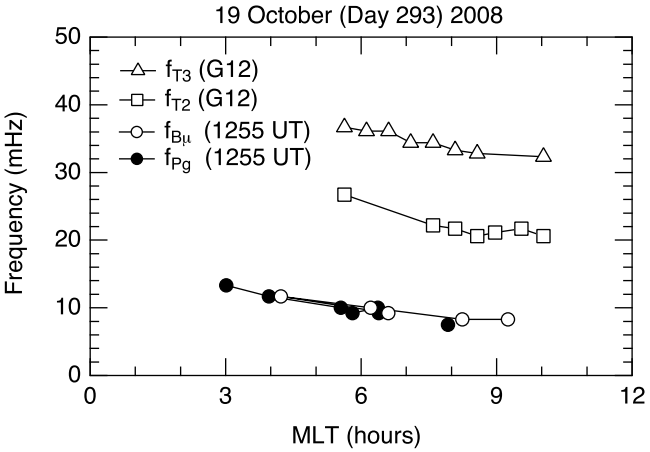

Figure 11. Composite plots of pulsation frequencies versus MLT for 19 October 2008. See text for explanation.

between 1245 and 1305 UT, when the foot point of THEMIS-A was close to GILL and both the satellite and the ground station detected strong ~10 mHz pulsations. The stacked line plots of GOES and ground data are ordered by MLT, with data from the earliest MLT plotted at the bottom. The GOES satellites span 5 h in MLT from ~0400 to ~0900, while THEMIS-A and the ground stations were near 0600 MLT. In the spectrum plots (right column), a vertical dashed line is drawn at the ground Pg frequency of 10 mHz.

[30] Both the time series and spectra indicate that there were pulsations at all locations but with some position dependencies. The satellite magnetic field shows oscillations in all three components, indicating that the pulsations are mixed in polarization with finite compressional and transverse components. The waveform is regular at each location but the amplitude varies. Also, the relative amplitude among the magnetic field components changes from one satellite to another. The wave frequency is nearly identical on the ground, at THEMIS-A, and at GOES-13, but it shows a systematic variation over the 5 h MLT range that was covered by the GOES satellites: the frequency decreases from 12 mHz at 4.22 h MLT (GOES-11) to 8 mHz at 9.25 h MLT (GOES-10).

[31] An interesting feature seen at GOES-11, closest to the equator (MLAT = 4.6°) among the GOES satellites, is the B_μ waveform that is not a perfect sinusoid. This waveform deformation produces evenly spaced spectral peaks at 12, 24, and 36 mHz. Waveform deformation is also visible in the THEMIS-A B_μ component. In this case, spectral peaks appear at 10 mHz and near its integral multiples. Waveform deformation similar to this has been reported for storm-time Pc5 waves [*Higuchi et al.*, 1986; *Takahashi et al.*, 1987] and is known as frequency doubling. Nonlinear mechanisms have been proposed to explain this phenomenon [*Higuchi et al.*, 1986; *Southwood and Kivelson*, 1997]. A similar process could be responsible for the 10 mHz pulsation reported here.

4.5. MLT Dependence of Frequency

[32] We examined the position dependence of pulsation frequency noted in Figure 10 using data from other locations and summarize the results in Figure 11. The data points labeled f_{Pg} are instantaneous Pg frequencies at 1255 UT observed at longitudinally separated ground stations, WHIT, FSIM, RABB, TPAS, FCHU, GILL, ISLL, and KUUJ (in increasing order of MLT). Similarly, the data points labeled $f_{B\mu}$ are instantaneous frequencies of compressional magnetic pulsations at 1255 UT observed at GOES-11, GOES-13, THEMIS-A, GOES-12, and GOES-10 (in increasing order of MLT). The data points labeled f_{T2} and f_{T3} are toroidal wave frequencies at the second and third harmonics observed by the GOES-12 satellite between 1015 and 1515 UT.

[33] Several features are obvious in Figure 11. First, the ground Pg frequency f_{Pg} depends on MLT. The frequency decreases monotonically from 13.3 mHz at 0300 MLT to 7.5 mHz at 0800 MLT. This MLT dependence has been noted previously [*Green*, 1979; *Brekke et al.*, 1987; *Thompson and Kivelson*, 2001] and appears to be a common feature. The $f_{B\mu}$ values almost perfectly match the f_{Pg} values, implying that these frequencies arise from the same wave mode. The toroidal harmonics also show a decreasing trend, which is very typical at geosynchronous orbit and can be explained by local time variation of mass density [*Takahashi and McPherron*, 1982]. The $f_{B\mu}/f_{T3}$ ratio at a given MLT is ~0.25, which is above the theoretical ratio of $f_{P1}/f_{T3} \sim 0.18$ [*Cummings et al.*, 1969], where f_{P1} is the fundamental frequency of the guided poloidal mode (we used a power law mass density model with the mass model exponent of 1.0, as will be discussed below). The discrepancy may lie in the fact that the theory assumes $|m| = \infty$ for the guided poloidal mode, whereas the observed Pg had a moderate value $m \sim -15$. If we use f_{T1}, which corresponds to $m = 0$, instead of f_{P1}, we get the frequency ratio $f_{T1}/f_{T3} \sim 0.24$, which is very close to the observed $f_{B\mu}/f_{T3}$ ratio. This result is strong evidence that the ground Pg signals originated from fundamental mode eigenoscillations of geomagnetic field lines.

4.6. R_{max} Dependence of Frequency

[34] Standing Alfvén wave frequency also varies with field line radial distance, and the radial frequency profile provides information on the source region of the Pg event. The open circles labeled $f_{E\phi}$ in Figure 12 indicate the frequency of the narrowband pulsations observed in the THEMIS-A E_ϕ component between 1200 and 1600 UT. The $f_{E\phi}$ data points cover both the short interval of close THEMIS-A and GILL conjunction (~1300 UT) as well as a long time interval following it (see Figure 9). The $f_{E\phi}$ value changed from 11 mHz at $R_{max} = 5.4$ to 4 mHz at $R_{max} = 9.6$. The only reasonable interpretation of the monotonically falling frequency is that the frequency represents the fundamental mode of local field line oscillation that existed over a wide range of R_{max}, essentially from the plasmapause to the magnetopause (magnetopause encounter occurred at 1732 UT, $R_{max} = 10.6$). Because the satellite moved only 1.9 h in MLT while moving outward from $R_{max} = 5.4$ to $R_{max} = 9.6$, we can ignore the MLT dependence of frequency to the first approximation and attribute the observed frequency change to the radial variation of the background magnetic field and the plasma mass density.

[35] Included in Figure 12 are the Pg frequencies (f_{Pg}) observed on the ground at GILL, RABB, and FCHU in the 1245–1305 UT data window. The ground frequency

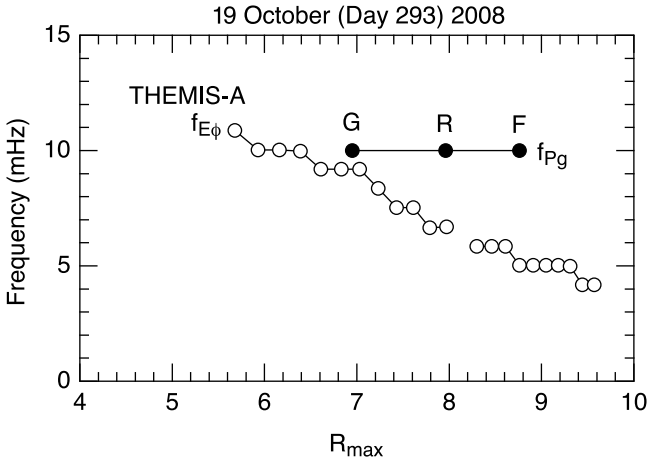

Figure 12. Pulsation frequency versus R_{max} on 19 October 2008. The open circles labeled $f_{E\phi}$ indicate the frequency at the most prominent peak in the power spectrum of the E_ϕ oscillations observed at THEMIS-A from 1220 UT (R_{max} = 5.43, MLT = 6.0 h) to 1600 UT (R_{max} = 9.57, MLT = 7.90 h). The solid circles labeled f_{Pg} indicate the frequency of the Pgs observed on the ground at GILL (G), RABB (R), and FCHU (F) between 1245 and 1305 UT.

(10 mHz) does not depend on R_{max}, in strong contrast to the frequency observed in the magnetosphere. f_{Pg} and $f_{E\phi}$ match at R_{max} = 6–7, implying that the source of ground Pg pulsations is located at this distance; that is, very near geostationary orbit.

4.7. MLAT Dependence of Amplitude

[36] Another way of determining the standing wave mode is to examine the variation of wave amplitude along the field line; that is, as a function of the latitudinal distance (MLAT) from the magnetic equator. We examine the B_v/B_μ amplitude ratio because the amplitude of individual field components will vary both with universal time and local time, but the ratio B_v/B_μ for a given MLAT value will not vary much as long as the standing wave mode remains the same. The key point here is the fact that, at the equator, an odd mode wave has a node of B_v and antinode of B_μ, whereas an even mode has an antinode of B_v and a node of B_μ (see Figure 2 for the mode structure of B_v). A small but finite compressional component B_μ should be present if the azimuthal wave number (m) is finite. Near the magnetic equator the B_v/B_μ amplitude ratio will be an increasing function of MLAT for odd mode waves, whereas the ratio will be a decreasing function for even mode waves.

[37] Figure 13 shows the B_v/B_μ amplitude ratio evaluated at the five satellites for 1245–1305 UT and plotted as a function of MLAT. For each component we integrated the PSD over the 5 mHz band centered on the spectral peak nearest the Pg frequency of 10 mHz and then took the square root of the integrated power to define the amplitude. Geostationary satellites are on the geographic equator, but the ~11° tilt of the dipole axis relative to the Earth's spin axis makes the satellite MLAT value vary from one geographic longitude to another. In the case of our Pg event the MLAT values at the GOES and THEMIS-A satellites ranged from ~4° to ~10°. Overall, the ratio clearly increases with MLAT, which is consistent with odd mode waves.

4.8. E and B Relationship at THEMIS-A

[38] Availability of both **E** and **B** field measurements in space allows us to do a variety of analyses. In Figure 14 we examine the relative phase and amplitude of E_ϕ, B_v, and B_μ to gain information on the propagation of the 10 mHz wave. The left column (Figure 14a) shows the relationship between E_ϕ and B_v and the right column (Figure 14b) the relationship between E_ϕ and B_μ. In each column, the time series is shown at the top, followed by the PSD, coherence, and phase delay as a function of frequency. In Figure 14a we find that B_v leads E_ϕ by 96° at 10 mHz, where the PSD is peaked. A phase difference that is close to 90° means a wave standing (rather than propagating) along the background magnetic field. Comparing the observed E_ϕ and B_v time series with the standing wave model illustrated in Figure 2, we find that an odd mode standing wave explains the observation. The amplitude of the oscillations also suggests an odd mode standing wave: the E_ϕ component exhibits large amplitude, ~8 mV/m peak-to-peak, while the B_v component exhibits small amplitude, ~0.8 nT peak-to-peak. The proximity of THEMIS-A to the magnetic equator (MLAT ~ 4°) means that the satellite was near the equatorial antinode (node) of E_ϕ (B_v). The amplitude of field line displacement in the radial direction, ξ_v, calculated from the observed electric field and the observed background magnetic field of 115 nT, is ~2200 km peak-to-peak. The phase and amplitude relationship for E_ϕ and B_v is discussed in more detail in the next section using a numerical model of standing Alfvén waves. The E_ϕ and B_μ data shown in Figure 14b are similar to Figure 14a, with an important difference in the phase, −123°. A phase value that is not close to ±90° means that the wave had an appreciable propagating component in the radial direction.

[39] Electromagnetic energy flow associated with the 10 mHz wave can be better seen in Figure 15, in terms of the Poynting vector $\mathbf{S} = \mathbf{E} \times \mathbf{B}$. Under the assumption $\mathbf{E}.\mathbf{B}_0 = 0$

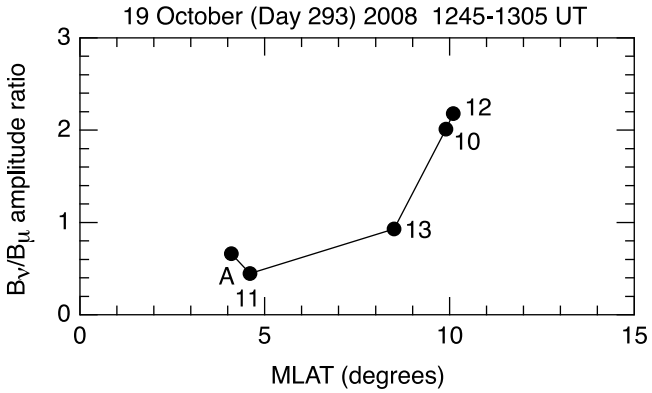

Figure 13. Magnetic latitude dependence of the B_v to B_μ amplitude ratio in the magnetosphere during a 20 min period on 19 October 2008, when there was a Pg activity on the ground. Contributing to the plots are observations from GOES-10 (10) through -13 (13) and THEMIS-A (A).

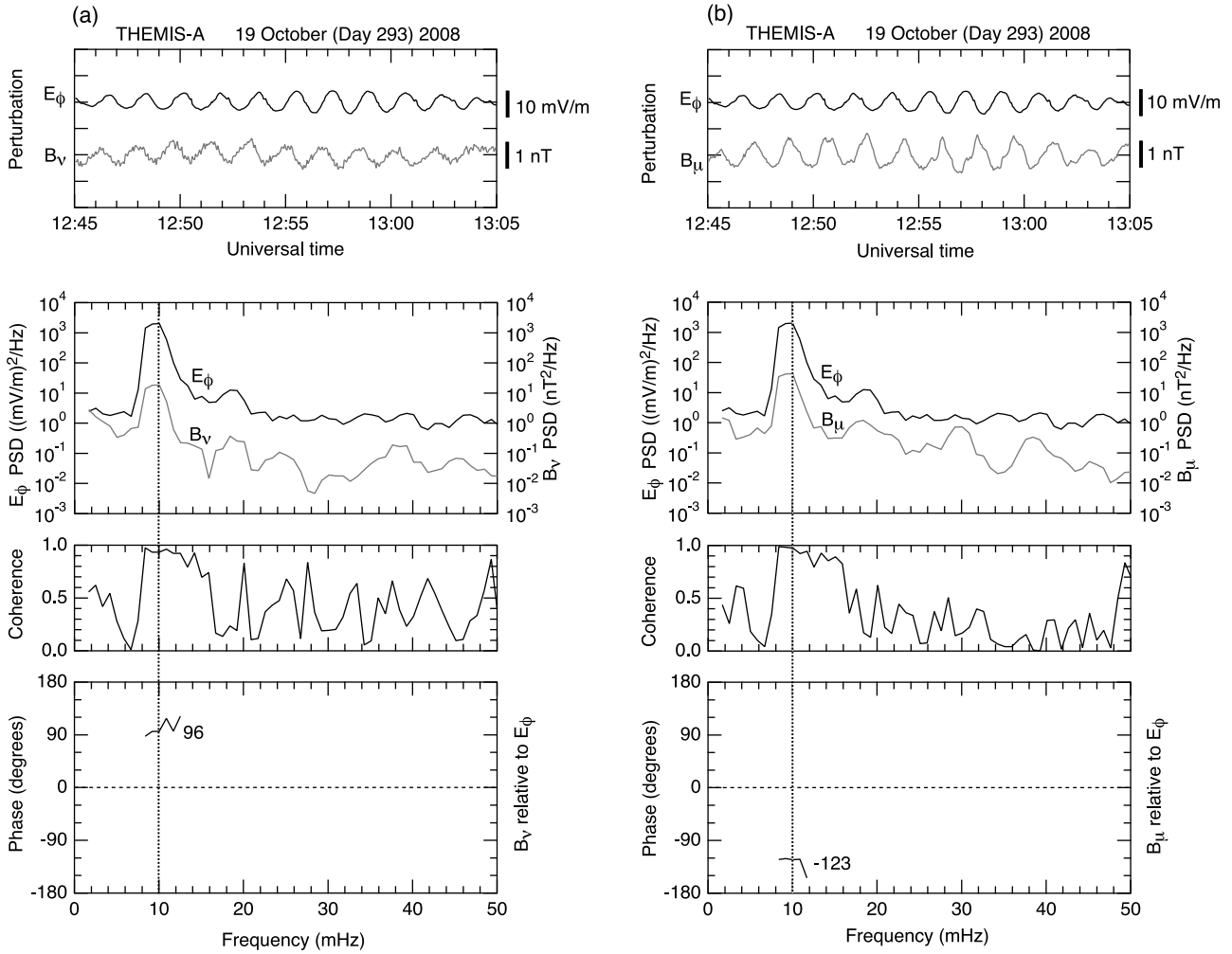

Figure 14. Relationship between two field components at THEMIS-A during the Pg event on 19 October 2008. (a) Results for E_ϕ and B_v. From top to bottom, time series, PSD, coherence, and phase difference. (b) Results for E_ϕ and B_μ.

(e.g., $E_\mu = 0$), **S** is given by $(E_\phi B_\mu, -E_v B_\mu, E_v B_\phi - E_\phi B_v)$. The field components entering the Poynting vector calculation were band-pass filtered with a passband of 8–12 mHz to remove variations that are slower or faster than the Pgs. The black line that bounds the shaded area indicates 200 s running averages of the Poynting flux, denoted $\langle \mathbf{S} \rangle$ below. Time averaging is useful when considering net energy flow associated with electromagnetic waves [e.g., *Cummings et al.*, 1978]. Figure 15a shows that $\langle S_v \rangle$ is shifted negative with a magnitude that is substantial relative to the overall variation of the unaveraged S_v. The negative value means net energy flow toward the Earth. This is potentially a very important piece of information when discussing the energy source of the Pg. By contrast, Figures 15b and 15c indicate that the magnitudes of $\langle S_\phi \rangle$ and $\langle S_\mu \rangle$ are smaller than that of $\langle S_v \rangle$, indicating that the wave was nearly nonpropagating (or standing) in the azimuthal direction and along the ambient magnetic field. However, we point out that $\langle S_\mu \rangle$ is positive around the peak (~1255 UT) of the pulsation amplitude, which means that energy flowed toward the northern ionosphere. Because the measurement was made slightly north of the magnetic equator, this flow direction is consistent with the ionosphere being the sink of the wave energy. Ionospheric damping of standing Alfvén waves is quantitatively described in section 5.1.

5. Discussion

5.1. Numerical Models of Standing Alfvén Waves

[40] The assumption made by most researchers is that Pgs are standing Alfvén waves. We demonstrate that this indeed is a valid assumption by comparing the observed properties of our Pg event with numerical standing Alfvén wave models. Based on the strong poloidal components observed by THEMIS-A and other satellites, we only consider the guided poloidal mode [*Radoski*, 1967]. We numerically solve the poloidal wave equation as formulated previously for a dipole magnetic field [*Westphal and Jacobs*, 1962; *Cummings et al.*, 1969; *Orr and Matthew*, 1971] and allow damping of the wave through ionospheric Joule dissipation. The damping is incorporated by imposing the boundary condition $B_v = \pm \Sigma_P E_\phi$ at the ionospheric foot points of the field line, where Σ_P is the height integrated Pedersen conductivity and the sign on the right-hand side of the equation is chosen to ensure that energy

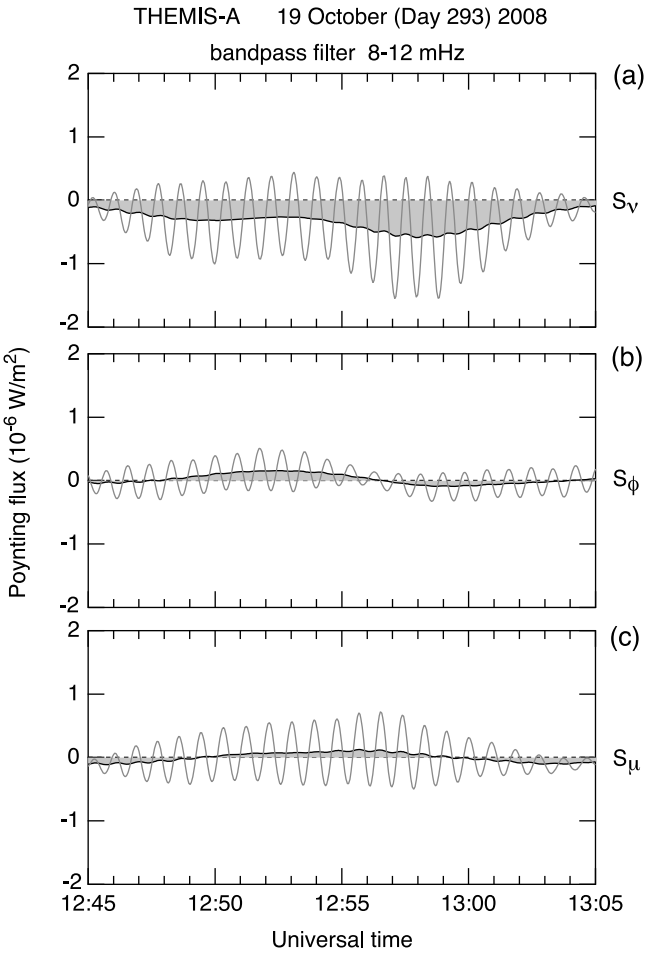

Figure 15. Poynting flux associated with the 10 mHz pulsation observed at THEMIS-A during the ground Pg activity on 19 October 2008. The flux was computed using filtered **E** and **B** field data with a passband of 8–12 mHz. (a) Radial component. (b) Azimuthal component. (c) Magnetic field aligned component.

(Poynting flux) flows from the magnetosphere to the ionosphere [*Newton et al.*, 1978; *Glassmeier et al.*, 1984]. Although it is quite obvious that our Pgs correspond to fundamental mode waves from comparison of their frequency with toroidal wave frequencies (Figure 11), we show numerical models of both the fundamental and second harmonic waves to strengthen our mode identification.

[41] In order to get the poloidal wave solution we need to specify the L shell, the mass density variation along the field line, and the conductivity at the ionospheric foot points of the field line. Because we are interested in explaining the **E** and **B** field oscillations at THEMIS-A, we choose $L = 6.5$ corresponding to the amplitude maximum at this spacecraft, which occurred at ~1255 UT. As for the density variation along the field line, we adopt the commonly used power law model, $\rho = \rho_{eq}(LR_E/R)^{\alpha}$, where ρ_{eq} is the equatorial mass density and R is geocentric distance along the field line. We choose $\alpha = 1.0$ based on recent studies of multiharmonic toroidal waves [e.g., *Takahashi and Denton*, 2007].

[42] The ionospheric conductivity is controlled by solar illumination and particle precipitation. To choose the value of Σ_P, we first determined the magnetic field line foot points of THEMIS-A using the T89c/IGRF magnetic field model for Kp = 2 and then determined the solar zenith angle at the foot points. The solar zenith angle was 91° at the northern foot point and 88° at the southern foot point, which means that the solar EUV radiation did not contribute to the conductivity. This led us to consider only particle precipitation as the controlling factor of the conductivity.

[43] The intensity of particle precipitation is highly variable both in time and space, so precise evaluation of the height integrated conductivity for our Pg event is difficult. Accordingly, we relied on the statistical results derived by *Hardy et al.* [1987] using measurements of the flux of precipitating particles. From Figure 2 of their paper we find that for Kp ~ 2 we have $\Sigma_P \sim 2$ S for the THEMIS-A foot points; that is, λ_{CGM} ~65°, MLT ~0600. This is the nominal Σ_P value that we use in computing the eigenmode structure of poloidal waves. We assume that Σ_P is the same between the northern and southern hemispheres, eliminating the possibility of the quarter wave mode field line oscillations [*Allan*, 1983].

[44] The real Σ_P value during the Pg event could differ from the statistical value, so we examined how the poloidal wave solutions depend on Σ_P. Figure 16 shows the fundamental (Figure 16a) and second harmonic (Figure 16b) poloidal mode frequencies as a function of Σ_P. Plotted are the real part f_r of the complex eigenfrequency ($2\pi f_r - i\gamma$) and the wave lifetime, $\tau (= f_r/\gamma)$, which is the amplitude e-folding time normalized to the wave period, that is, the number of wave cycles it takes for the amplitude to decrease by a factor of e [*Takahashi et al.*, 1996]. For each harmonic mode, we set ρ_{eq} at the value that gives $f_r = 10.0$ mHz at the limit of $\Sigma_P = \infty$. This density is 1.93 amu.cm^{-3} for the fundamental mode and 23.2 amu.cm^{-3} for the second harmonic. We note that the electron density n_e inferred from the THEMIS-A spacecraft potential was 1.1 cm^{-3}, which means average ion mass M ($= \rho/n_e \sim \rho_{eq}/n_e$) has to have a value of ~1.8 amu for the fundamental mode and ~22 amu for the second harmonic. Whereas the former M value is physically possible (M should lie between 1 and 16 amu for plasma consisting of H^+, He^+, and O^+) and in line with statistical studies [*Takahashi et al.*, 2006; *Denton et al.*, 2011], the latter M value exceeds the physical limit and is impossible. This is another piece of evidence for the fundamental mode.

[45] Figure 16a shows that the fundamental mode is completely damped and f_r approaches zero for $\Sigma_P = 0.23$ S. For the more realistic value of $\Sigma_P \sim 2$ S, f_r is very close to that for $\Sigma_P = \infty$ while damping is still severe ($\tau \sim 1$). If $\Sigma_P \sim 2$ S is close to the reality, this theoretical result means that free energy was continuously fed to the wave in order to sustain oscillations for many cycles. Alternatively, we could argue that the actual height integrated conductivity was much higher, $\Sigma_P \sim 10$ S for example, in which case the wave lifetime increases to ~10 and the wave can be sustained without strong energy input. The second harmonic mode (Figure 16b) does not suffer complete damping at low Σ_P, but its frequency properties for $\Sigma_P > 1$ S are qualitatively very similar to those of the fundamental mode.

[46] Our choice of $\alpha = 1.0$ for the mass distribution along the field line was based on statistical studies of toroidal harmonics, but the density model may not be accurate for a particular wave event. Given the uncertainty of the mass distribution, we repeated the calculation of the standing wave

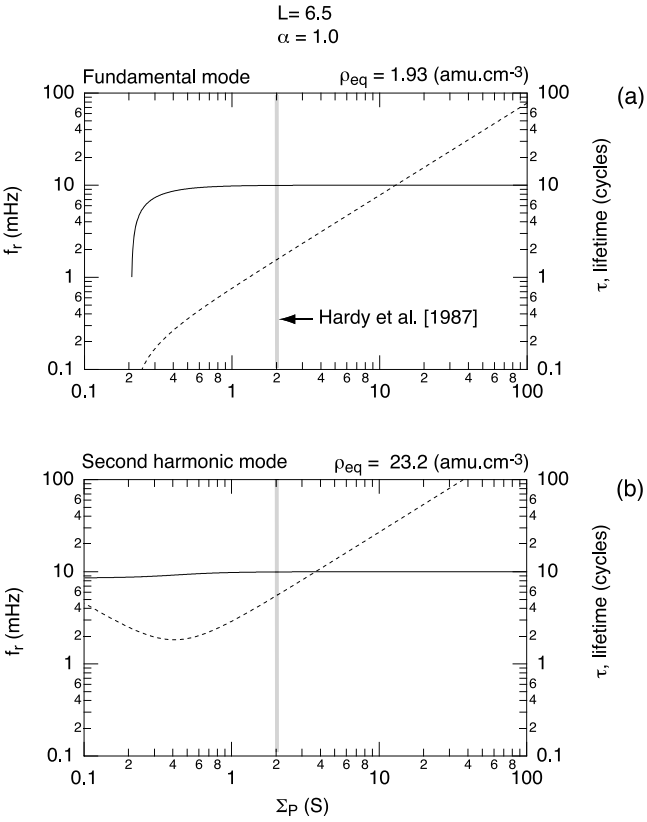

Figure 16. Frequency and lifetime of the poloidal mode oscillation on a dipole field line at $L = 6.5$ versus height integrated Pedersen conductivity at the field line foot points. The solid line is the real part of the frequency, with the scale given on the left. The dashed line is the amplitude *e*-folding time normalized to the wave period, with the scale given on the right. The value of the equatorial mass density ρ_{eq} is chosen so that that the wave equation gives the frequency of 10 mHz at the limit of $\Sigma_P = \infty$. (a) Results for the fundamental (odd, symmetric) mode. (b) Results for the second harmonic (even, antisymmetric) mode.

models using different values of α. In the literature α in the range of 0–6 has been used [e.g., *Cummings et al.*, 1969]. If we use $\alpha = 6$, the equatorial mass density is lowered to 1.34 amu.cm^{-3} for the fundamental mode and 9.78 amu.cm^{-3} for the second harmonic, corresponding to $M \sim 1.2$ amu and $M \sim 8.9$ amu, respectively. The former M value is reasonable for the H^+-dominated plasma in the plasma trough at the solar minimum [*Denton et al.*, 2011], but the latter M value is not. Therefore, the uncertainty in the mass density model does not affect our conclusion that the Pg was an odd mode wave.

[47] The field line mode structure of the two harmonic modes for $\Sigma_P = 2$ S is shown in Figure 17. We have included the results for $\Sigma_P = \infty$ (dashed line) as a reference. For the $\Sigma_P = 2$ S case there is substantial E_ϕ amplitude at the ionospheric foot points and in their vicinity. Nearer the magnetic equator, however, the E_ϕ mode structure becomes very close to that for $\Sigma_P = \infty$. By contrast, the B_v mode structure is very similar all along the field line between the two Σ_P values.

[48] Even though the THEMIS-A observation was made at a single point in MLAT (~4° north), availability of both E_ϕ and B_v data gives conclusive evidence for the fundamental mode in terms of field line mode structure. In Figure 17a we find that the fundamental mode has a B_v node at the equator, which produces an equatorial minimum in the B_v/E_ϕ amplitude ratio and a 180° shift in the relative phase between E_ϕ and B_v across the magnetic equator. At the THEMIS-A latitude, the amplitude ratio is 0.06 (nT/(mV/m)) and the phase delay is 96° (B_v leads E_ϕ by approximately a quarter of a wave period). Going back to THEMIS-A observations (Figure 14), we find that the peak-to-peak amplitude was $B_v \sim 0.8$ nT and $E_\phi \sim 8$ mV/m, which gives $B_v/E_\phi \sim 0.1$, and that B_v led E_ϕ by ~96° (Figure 14). Both the amplitude ratio and phase delay are close to the model values.

[49] Figure 17b indicates a totally different story for the second harmonic. For this mode the B_v (E_ϕ) component has an antinode (node) at the equator, producing a large B_v/E_ϕ ratio of 5.3 and a $B_v - E_\phi$ phase delay of −92° at the THEMIS-A latitude. These are very different from the observed values and we can dismiss the second harmonic wave as the source of the observed Pgs.

[50] We also computed the eigenmode structure for the ionospheric height integrated conductivity based on the International Reference Ionosphere (IRI) as was done by *Glassmeier et al.* [1999] for a Pg event. Using the online software provided by the World Data Center for Geomagnetism, Kyoto (http://wdc.kugi.kyoto-u.ac.jp/), we found that the IRI-based height integrated Pedersen conductivity is 1.3 S at the southern foot point and 0.77 S at the northern foot point. For the fundamental mode, the lower Σ_P values and the north-south asymmetry produce some north-south asymmetry of E_ϕ and increase the $E_\phi - B_v$ phase lag at the THEMIS-A position to 128° from 96° that is found in Figure 16a. However, the mode frequency and the wave structure near the THEMIS position differ very little from the results shown in Figure 16a.

[51] The THEMIS-A latitude of 4° means that the small shift of the equatorial node of the B_v component, which can be caused by the difference in Σ_P between south and north [*Allan*, 1983], can impact our interpretation of the wavefields. If the node is shifted northward by more than the 4°, our argument for the fundamental mode is not valid. To demonstrate that the node is not shifted much for realistic Σ_P values, we show in Figure 18 the magnetic latitude of the B_v node as a function of the height integrated conductivity at south (Σ_{PS}) and north (Σ_{PN}). To generate this figure we solved the poloidal wave equation for the fundamental mode, assuming $L = 6.5$, $\alpha = 1.0$, and $\rho_{eq} = 1.93$ amu.cm^{-3}. The node is defined to be the location where B_v exhibits a minimum. Contours are drawn for a node located at MLAT = 0, ±1°, and ±4°. The node is located at MLAT = 0 when $\Sigma_{PS} = \Sigma_{PN}$, as should be the case, whereas it is located north of the equator (MLAT > 0) when $\Sigma_{PS} > \Sigma_{PN}$. For the height integrated conductivities derived from the IRI model (diamond), the node is located at MLAT = 0.2°, very close to the equator. To move the node to the satellite location of MLAT = 4°, the Σ_{PN} value has to be ~0.3 S, which is unrealistically low. We conclude that the model shown in Figure 17a is valid concerning the location of the B_v node.

[52] Finally, we can estimate the magnetic field amplitude at the ionospheric foot points from the numerical models and discuss how it relates to the amplitude on the ground. Noting that Figure 17 shows results derived for the assumed B_v amplitude of 1.0 nT at the foot point, we find that the observed E_ϕ RMS amplitude 2.6 mV/m at the peak of the poloidal

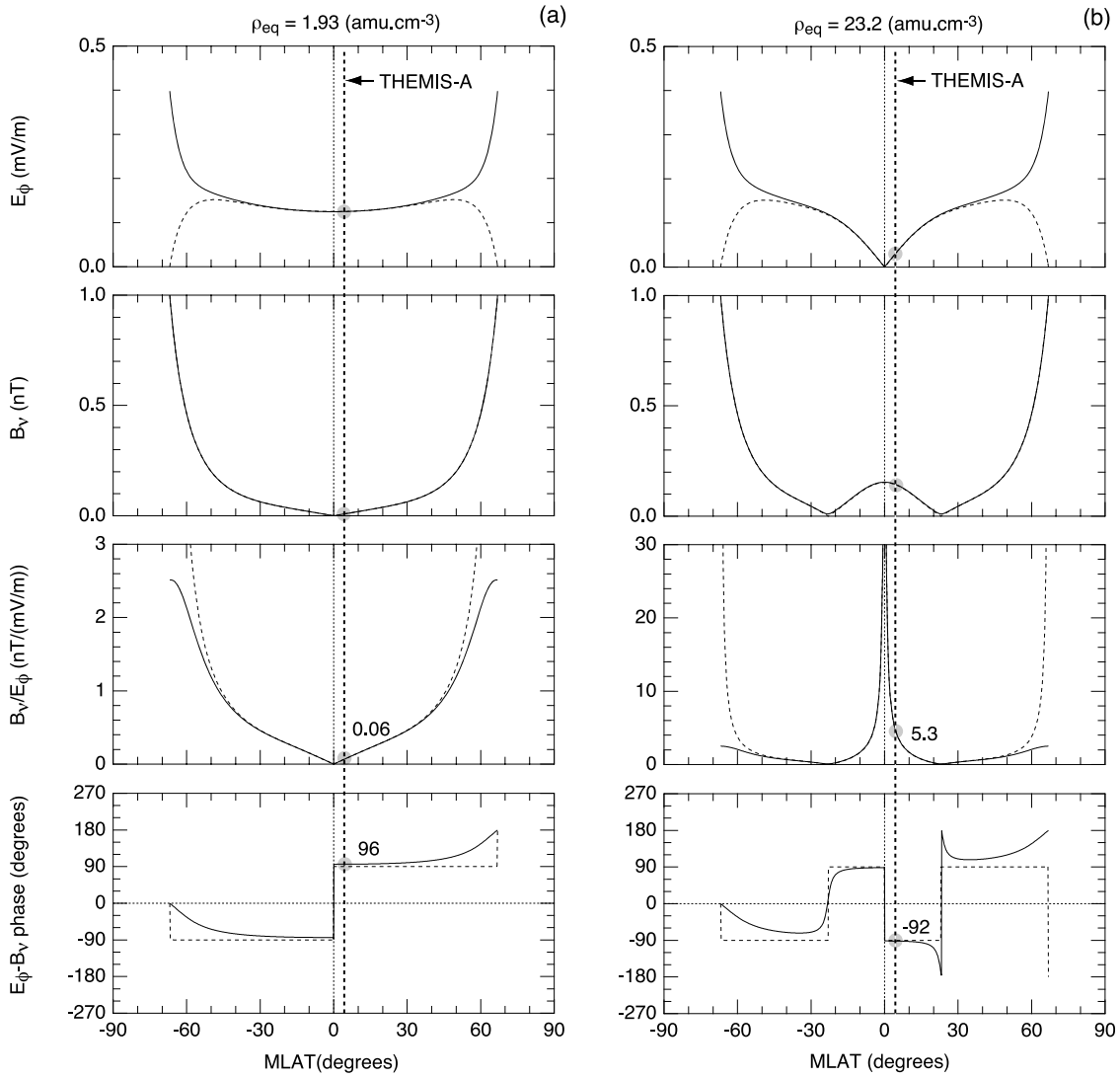

Figure 17. Numerically obtained poloidal mode structure along a dipole field line, plotted as a function of magnetic latitude. The field line is located at $L = 6.5$ and the height integrated ionospheric conductivity Σ_P is 2 S at both ionospheric foot points of the field line. The value of the equatorial mass density ρ_{eq} is chosen so that the wave equation gives the frequency of 10 mHz at the limit of $\Sigma_P = \infty$. The magnetic field amplitude B_v is chosen to be 1 nT at the field line foot points, and the corresponding electric field amplitude E_ϕ is given in units of mV/m. The vertical dashed line drawn at MLAT = 4° indicates the location of THEMIS-A at 1255 UT on 19 October 2008. (a) Results for the fundamental (odd, symmetric) mode. (b) Results for the second harmonic (even, antisymmetric) mode.

oscillations observed by THEMIS-A (Figure 7b) near the magnetic equator corresponds to estimated B_v RMS amplitude of 21 nT at the ionospheric foot point. The Y RMS amplitude of 3.7 nT observed on the ground at CARISMA-GILL near the foot point of THEMIS-A (Figure 7b) is only ~18% of the estimated B_v amplitude at the ionosphere, which means that a strong attenuation of the amplitude occurred between the ionosphere and the ground.

[53] Ionospheric attenuation of Alfvén waves can be estimated using a well-known formula for ionospheric screening of MHD waves [*Hughes and Southwood*, 1976; *Nishida*, 1978; *Glassmeier*, 1984; *Yeoman et al.*, 2006]. For the poloidal wave under consideration, the formula predicts the amplitude ratio $Y/B_v = (\Sigma_H/\Sigma_P)\exp(-kh)$, where B_v is evaluated at the ionosphere, Σ_H is the height integrated Hall conductivity, k is the horizontal wave number at the ionosphere, and h is the effective height of the ionosphere (~120 km). We adopt $\Sigma_H/\Sigma_P \sim 2$ following *Hardy et al.* [1987] and assume k to be given in the form $k = (k_x^2 + k_y^2)^{1/2}$ in terms of the latitudinal and longitudinal wave numbers k_x and k_y. The wavelength λ is related to k as $k = 2\pi/\lambda$. For our Pg event we have $m \sim -15$, which translates to a longitudinal wavelength λ_y ~1000 km at the ionospheric height. The above formula then indicates that we need a latitudinal wave number $\lambda_x \sim$ 400 km to achieve the Y/B_v amplitude ratio of 0.18. If this is the case, the latitudinal scale size of the pulsation was a few degrees, which is comparable to the statistical result reported by *Chisham et al.* [1997]. Note that the formula quoted above

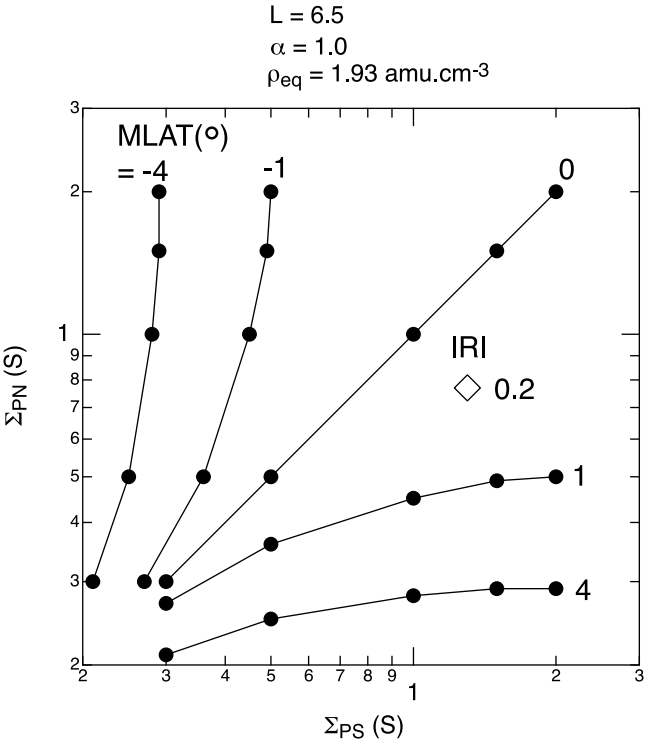

Figure 18. Location (MLAT) of the node of the B_v component for the model fundamental poloidal wave as a function of the height integrated Pedersen conductivity at the ionospheric foot points of the field line that sustains the wave. The height integrated conductivities at south (Σ_{PS}) and north (Σ_{PN}) are taken as independent variables and contour lines are used to indicate the values of Σ_{PS} and Σ_{PN} for the node location of MLAT = 0, ±1°, and ±4°. Dots indicate the Σ_{PS} and Σ_{PN} values with which the numerical calculation was done assuming $L = 6.5$, $\alpha = 1.0$, and $\rho_{eq} = 1.93$ amu.cm^{-3}. The diamond indicates the Σ_{PS} and Σ_{PN} values derived from the IRI model, which give the node at MLAT = 0.2°.

assumes a periodic wave structure both in latitude and longitude, whereas the latitudinal structure of geomagnetic pulsations is not periodic. Therefore, the discussion presented here should be taken as a rough approximation.

5.2. MLT Dependence of Pg Frequency

[54] We observed an MLT dependence of Pg frequency similar to that reported previously (*Thompson and Kivelson* [2001] and references therein). In our event, the ground Pg frequency (at a given UT epoch) varied from 13.3 mHz at 0300 MLT to 7.5 mHz at 0800 MLT and matched the frequency of poloidal oscillations with a small but finite compressional component at geostationary orbit (Figure 11). This implies that the ground Pg signals originated from the poloidal oscillations in space that are excited on field lines at $L \sim 7$. If this is the case, the MLT dependence of Pg frequency is attributed to the MLT dependence of the frequency of standing Alfvén waves at $L \sim 7$. This interpretation is rather straightforward in view of the statistical studies reporting that the frequency of toroidal waves at geostationary orbit decreases with MLT during daytime hours [*Takahashi and McPherron*, 1984]. The standing wave frequency, regardless of poloidal or toroidal polarization, decreases because mass loading from the ionosphere continues from the time the magnetic flux tube emerges from the nightside (at dawn) until the time flux tube returns to the nightside (at dusk).

[55] If the above interpretation is correct, then we encounter another fundamental question: why is the $L \sim 7$ region special? Standing field line oscillations can be excited anywhere in the magnetosphere as long as the ionosphere provides appropriate boundary conditions. According to Figures 12 and 16, standing field line oscillations were continuously present at THEMIS-A from $R_{max} = 5.6$ to $R_{max} = 9.6$, implying that the ionospheric height integrated conductivity was high enough to sustain standing oscillations well inside and outside of the region, with a strong Pg signal located at $R_{max} \sim 7$. There are at least two possible answers to the above question. One is that strong odd mode poloidal waves are excited preferentially at $L \sim 7$; that is, ULF plasma instability occurs on a thin L shell at a fixed distance. *Chisham* [1996] and *Ozeke and Mann* [2001] presented a model calculation to show that an unstable ion energy distribution emerges during geomagnetically quiet periods because of the energy dependence of ion drift orbits. Although this calculation was done to explain the generation of second harmonic waves, we speculate that a similar scenario can explain the formation of an unstable particle population that leads to generation of odd mode waves.

[56] The other possibility is that fundamental poloidal waves are excited on various L shells but that only those near $L = 7$ propagate to the ground. It is well known that high m Alfvén waves propagating from the magnetosphere are attenuated on the ground level because of ionospheric screening [*Hughes and Southwood*, 1976]. Therefore, if the m value of the fundamental poloidal waves becomes large (~100) and invisible to ground magnetometers away from $L \sim 7$, then we do not have to limit the instability region to a thin L shell at a fixed distance. High m waves invisible to ground magnetometers have been observed with ionospheric radar [*Yeoman et al.*, 2000; *Baddeley et al.*, 2002, 2005b]. One such wave occurred near noon and had a frequency consistent with the fundamental poloidal mode [*Yeoman and Wright*, 2001]. In addition, the wave had an azimuthal wave number of ~−35 (westward propagation), which was large enough to cause strong attenuation of the wave at the ground level. It is quite plausible that fundamental poloidal waves are commonly excited in the magnetosphere, but only a fraction of these have small enough m to propagate to the ground.

5.3. Drift Resonance

[57] The unambiguous information on the standing wave mode on the Pg event on 19 October 2008 imposes a strong constraint on the possible generation mechanism of the pulsation. Among the previous studies that identified odd mode waves, *Green* [1979, 1985] considered drift wave instability of the compressional Alfvén wave [*Hasegaw*a, 1971] as a possible source mechanism, whereas *Takahashi et al.* [1992] and *Thompson and Kivelson* [2001] considered drift resonance $\omega - m\omega_d = 0$ as the mechanism. The latter is a special case of energetic particle drift-bounce resonance with standing Alfvén waves [e.g., *Southwood*, 1976]. We concur with these studies and suggest that the possible generation mechanisms be pursued through analysis of relevant particle

data and numerical modeling of ring current ions in realistic magnetospheric magnetic field and electric field.

[58] In applying the drift wave instability theory [*Hasegawa*, 1971] to Pgs, *Green* [1979, 1985] pointed out that presence of cold plasma is necessary for the instability to occur. This would be possible if the waves are excited in the plasmasphere or in the region of detached ionospheric plasma (or drainage plumes). However, in the present study, the electron density data from THEMIS-A (Figure 7a) indicate that the Pgs were excited outside the plasmasphere. Therefore, it appears that the cold plasmaspheric plasma was effective in suppressing (rather than enhancing) the poloidal waves. For this reason, we do not consider the drift wave instability to be a likely source mechanism for the Pg event we studied.

[59] Concerning the drift resonance mechanisms, we find, on the basis of the formula by *Hamlin et al.* [1961], that 270 keV equatorial ions (pitch angle = 90°) are in resonance with a ULF wave having the properties observed by THEMIS-A during the Pg event: $L = 6.5$, $f = 10$ mHz, and $m = -15$. Note that with the solar illumination nearly the same at the northern and southern field line foot points (see section 5.1), it is unlikely that there was significant breakdown of the North-South symmetry of the wavefield that warrants modification [*Glassmeier et al.*, 1999; *Mann and Chisham*, 2000] of the standard formulation of drift-bounce resonance [e.g., *Southwood*, 1976]. Given a poloidal wavefield, there always will be a population of particles that satisfy the resonance condition, so the important question is whether the resonance acts as a channel through which net particle energy is transferred to the waves. According to *Southwood* [1976], an ion distribution function f satisfying $\partial f/\partial L|_{\mu,J} < 0$ can destabilize odd mode waves through drift resonance, where μ (not to be confused with the suffix for the **E** and **B** field components along the magnetic field) and J are the first and second adiabatic constants of particle motion.

[60] We note that the magnitude of m of our Pg event, 15, is near the lower end of the distribution of the statistical range 16–35 reported previously. This means that the energy (270 keV) of drift resonant ions derived above is higher than that for Pg events with more typical m values. For example, *Thompson and Kivelson* [2001] estimated the resonance energy to be in the range 100–150 keV for a Pg event with $m = -20$. Whether Pg events are excited by the same drift resonance mechanism over a wide range of ion energy needs to be addressed in the future.

5.4. Solar Cycle Variation of Standing Alfvén Wave Frequency

[61] One might wonder whether there are even mode Pgs. Considering the fact that all Pg studies that included satellite measurements favored odd mode waves, it is highly unlikely that even mode waves produce Pg signals on the ground. Then why were the even mode waves favored in some studies? We can offer an answer to this question concerning studies that used Pg frequency to infer the Pg standing wave mode. For example, *Chisham and Orr* [1991] compared Pg frequencies (~10 mHz, or period ~100 s) with the fundamental field line resonance frequencies reported in other studies. Specifically, these authors noted that Pg frequencies were much higher than the frequency of Pc4–5 pulsations that were reported by *Samson and Rostoker* [1972] and *Poulter et al.* [1984] at similar latitudes. Under the assumption that the Pc4–5 pulsations resulted from fundamental standing Alfvén waves, Chisham and Orr argued that the Pg pulsations originate from second harmonic standing waves.

[62] Implicit in the above argument is the assumption that the Alfvén wave frequencies did not change much among the studies. However, magnetospheric mass density exhibits a pronounced solar cycle variation and causes a variation in standing Alfvén wave frequencies. In a recent statistical study, *Takahashi et al.* [2010] demonstrated that toroidal wave frequencies at geostationary orbit change by a factor of ~2 over a solar cycle. The lowest frequencies occur at the solar maximum when the elevated solar EUV flux maximizes the density of the ionospheric ions (O^+ in particular) in the magnetosphere [*Denton et al.*, 2011]. The opposite, the lowest density and the highest frequencies, occurs at the solar minimum.

[63] To infer the harmonic mode for Pgs correctly, we need to know the fundamental Alfvén frequency at the solar minima, because Pgs are observed almost exclusively in a few-year period surrounding the minima [*Brekke et al.*, 1987]. It turns out that the statistics by *Samson and Rostoker* [1972] and *Poulter et al.* [1984] used data taken from periods of high solar activity, meaning that their pulsation frequencies were biased toward lower values. The fundamental mode frequencies reported by these authors should be raised by a factor of ~2 to be compared with Pg frequencies. If we do that, then the field line fundamental frequencies become closer to the Pg frequencies, which resolves much of the odd mode versus even mode controversy.

6. Conclusions

[64] We have studied the magnetic and electric field properties of magnetospheric ULF waves observed by five satellites during a period of Pg activity on the ground. The spacecraft were magnetically connected to the ground Pg activity, and all aspects of satellite observations indicate that the source of the Pgs was poloidal standing Alfvén waves with an odd (fundamental) mode structure along the field line. We have obtained additional information on the poloidal waves, including their spatial properties relative to the plasmapause and the Poynting flux associated with the waves. While we believe that the standing wave mode of Pgs is now firmly established, we recognize that there still remains the question of how the odd-mode poloidal waves are excited. Although we speculate that drift resonance is involved in the excitation of the waves, it is a totally unresolved question as to why the unstable particle population is formed at a particular solar activity phase, season, and local time.

[65] **Acknowledgments.** K.T. is grateful to Pat Newell, Richard Denton, Simon Wing, and Jesper Gjerloev for valuable discussion. We thank the Space Physics Group at the University of Alberta (Ian Mann, PI) for providing the CARISMA magnetometer data. Work at The Johns Hopkins University Applied Physics Laboratory was supported by NASA grant NNX10AK93G. The work by K.-H.G. was financially supported by the German Ministerium für Wirtschaft und Technologie and the Deutsches Zentrum für Luft und Raumfahrt under grant 50QP0402.

[66] Robert Lysak thanks the reviewers for their assistance in evaluating this paper.

References

Allan, W. (1983), Quarter-wave ULF pulsations, *Planet. Space Sci.*, *31*(3), 323–330, doi:10.1016/0032-0633(83)90083-1.

Annexstad, J. O., and C. R. Wilson (1968), Characteristics of Pg micropulsations at conjugate points, *J. Geophys. Res.*, *73*, 1805–1818, doi:10.1029/JA073i005p01805.

Auster, H. U., et al. (2008), The THEMIS fluxgate magnetometer, *Space Sci. Rev.*, *141*, 235–264, doi:10.1007/s11214-008-9365-9.

Baddeley, L. J., T. K. Yeoman, D. M. Wright, J. A. Davies, K. J. Trattner, and J. L. Roeder (2002), Morning sector drift-bounce resonance driven ULF waves observed in artificially induced HF radar backscatter, *Ann. Geophys.*, *20*, 1487–1498, doi:10.5194/angeo-20-1487-2002.

Baddeley, L. J., T. K. Yeoman, D. M. Wright, K. J. Trattner, and B. J. Kellet (2005a), On the coupling between unstable magnetospheric particle populations and resonant high m ULF wave signatures in the ionosphere, *Ann. Geophys.*, *23*, 567–577, doi:10.5194/angeo-23-567-2005.

Baddeley, L. J., T. K. Yeoman, and D. M. Wright (2005b), HF Doppler sounder measurements of the ionospheric signatures of small scale ULF waves, *Ann. Geophys.*, *23*(5), 1807–1820, doi:10.5194/angeo-23-1807-1820.

Barfield, J. N., L. J. Lanzerotti, C. G. Maclennan, G. A. Paulikas, and M. Schultz (1971), Quiettime observation of a coherent compressional Pc-4 micropulsation at synchronous altitude, *J. Geophys. Res.*, *76*, 5252–5258, doi:10.1029/JA076i022p05252.

Birkeland, K. (1901), Expédition Norvégienne de 1899–1990 pour l'étude des aurores boréalres. Résultats des recherches magnétiques, *Videnskabsselsk. Skr, I. Mat. Naturvidensk. K.*, *1*, 1–80.

Bonnell, J. W., F. S. Mozer, G. T. Delory, A. J. Hull, R. E. Ergun, C. M. Cully, V. Angelopoulos, and P. R. Harvey (2008), The Electric Field Instrument (EFI) for THEMIS, *Space Sci. Rev.*, *141*, 303–341, doi:10.1007/s11214-008-9469-2.

Brekke, A., T. Feder, and S. Berger (1987), Pc4 giant pulsations recorded in Tromsø, 1929–1985, *J. Atmos. Terr. Phys.*, *49*, 1027–1032, doi:10.1016/0021-9169(87)90109-7.

Chen, L., and A. Hasegawa (1991), Kinetic theory of geomagnetic pulsations, 1, Internal excitation by energetic particles, *J. Geophys. Res.*, *96*, 1503–1512, doi:10.1029/90JA02346.

Cheng, C. Z., Q. Qian, K. Takahashi, and A. T. Y. Lui (1994), Ballooning-mirror instability and internally driven Pc4–5 wave events, *J. Geomag. Geoelectr.*, *46*, 997–1009, doi:10.5636/jgg.46.997.

Chisham, G. (1996), Giant pulsations: An explanation for their rarity and occurrence during geomagnetically quiet times, *J. Geophys. Res.*, *101*, 24,755–24,763, doi:10.1029/96JA02540.

Chisham, G., and D. Orr (1991), Statistical studies of giant pulsations (Pgs): Harmonic mode, *Planet. Space Sci.*, *39*(7), 999–1006, doi:10.1016/0032-0633(91)90105-J.

Chisham, G., M. J. Taylor, and H. Luhr (1990), The magnetic and optical signature of a Pg pulsation, *Planet. Space Sci.*, *38*(11), 1443–1456, doi:10.1016/0032-0633(90)90119-B.

Chisham, G., D. Orr, and T. K. Yeoman (1992), Observations of a giant pulsation across an extended array of ground magnetometers and on auroral radar, *Planet. Space Sci.*, *40*(7), 953–964, doi:10.1016/0032-0633(92)90135-B.

Chisham, G., I. R. Mann, and D. Orr (1997), A statistical study of giant pulsation latitudinal polarization and amplitude variation, *J. Geophys. Res.*, *102*, 9619–9629, doi:10.1029/97JA00325.

Cummings, W. D., R. J. O'Sullivan, and P. J. Coleman Jr. (1969), Standing Alfvén waves in the magnetosphere, *J. Geophys. Res.*, *74*, 778–793, doi:10.1029/JA074i003p00778.

Cummings, W. D., S. E. DeForest, and R. L. McPherron (1978), Measurements of the Poynting vector of standing hydromagnetic waves at geosynchronous orbit, *J. Geophys. Res.*, *83*, 697–706, doi:10.1029/JA083iA02p00697.

Denton, R. E., M. F. Thomsen, K. Takahashi, R. R. Anderson, and H. J. Singer (2011), Solar cycle dependence of bulk ion composition at geosynchronous orbit, *J. Geophys. Res.*, *116*, A03212, doi:10.1029/2010JA016027.

Glassmeier, K.-H. (1980), Magnetometer array observations of a giant pulsation event, *J. Geophys.*, *48*, 127–138.

Glassmeier, K.-H. (1984), On the influence of ionospheres with non-uniform conductivity distribution on hydromagnetic waves, *J. Geophys.*, *54*, 125–137.

Glassmeier, K.-H., H. Volpers, and W. Baumjohann (1984), Ionospheric Joule dissipation as a damping mechanism for high latitude ULF pulsations: Observational evidence, *Planet. Space Sci.*, *32*, 1463–1466, doi:10.1016/0032-0633(84)90088-6.

Glassmeier, K.-H., S. Buchert, U. Motschmann, A. Korth, and A. Pederson (1999), Concerning the generation of geomagnetic giant pulsations by drift-bounce resonance ring current instabilities, *Ann. Geophys.*, *17*, 338–350, doi:10.1007/s00585-999-0338-4.

Green, C. A. (1979), Observations of Pg ULF pulsations in the northern auroral zone and at lower latitude conjugate regions, *Planet. Space Sci.*, *27*, 63–77, doi:10.1016/0032-0633(79)90148-X.

Green, C. A. (1985), Giant pulsations in the plasmasphere, *Planet. Space Sci.*, *33*(10), 1155–1168, doi:10.1016/0032-0633(85)90073-X.

Hamlin, D. A., R. Karplus, R. C. Vik, and K. M. Watson (1961), Mirror and azimuthal drift frequencies for geomagnetically trapped particles, *J. Geophys. Res.*, *66*, 1–4, doi:10.1029/JZ066i001p00001.

Hardy, D. A., M. S. Gussenhoven, R. Raistrick, and W. J. McNeil (1987), Statistical and functional representations of the pattern of auroral energy flux, number flux, and conductivity, *J. Geophys. Res.*, *92*, 12,275–12,294, doi:10.1029/JA092iA11p12275.

Hasegawa, A. (1971), Drift wave instability at the plasmapause, *J. Geophys. Res.*, *76*, 5361–5364, doi:10.1029/JA076i022p05361.

Higuchi, T., S. Kokubun, and S. Ohtani (1986), Harmonic structure of compressional Pc5 pulsations at synchronous orbit, *Geophys. Res. Lett.*, *13*(11), 1101–1104, doi:10.1029/GL013i011p01101.

Hillebrand, O., J. Münch, and R. K. McPherron (1982), Ground-satellite correlative study of a giant pulsation event, *J. Geophys.*, *51*, 129–140.

Hughes, W. J., and D. J. Southwood (1976), The screening of micropulsation signals by the atmosphere and ionosphere, *J. Geophys. Res.*, *81*, 3234–3247, doi:10.1029/JA081i019p03234.

Hughes, W. J., D. J. Southwood, B. Mauk, R. L. McPherron, and J. N. Barfield (1978), Alfvén waves generated by an inverted plasma energy distribution, *Nature*, *275*, 43–45, doi:10.1038/275043a0.

Kokubun, S. (1980), Observations of Pc pulsations in the magnetosphere: Satellite-ground correlation, *J. Geomag. Geoelectr.*, *32*(SII), 17–39.

Kokubun, S., K. N. Erickson, T. A. Fritz, and R. L. McPherron (1989), Local time asymmetry of Pc 4–5 pulsations and associated particle modulations at synchronous orbit, *J. Geophys. Res.*, *94*, 6607–6625, doi:10.1029/JA094iA06p06607.

Lanzerotti, L. J., and N. A. Tartaglia (1972), Propagation of a magnetospheric compressional waves to the ground, *J. Geophys. Res.*, *77*, 1934–1940, doi:10.1029/JA077i010p01934.

Li, W., et al. (2010), THEMIS analysis of observed equatorial electron distributions responsible for the chorus excitation, *J. Geophys. Res.*, *115*, A00F11, doi:10.1029/2009JA014845.

Mann, I. R., and G. Chisham (2000), Comment on "Concerning the generation of geomagnetic giant pulsations" by K.-H. Glassmeier et al., *Ann. Geophys.*, *18*, 161–166, doi:10.1007/s005850050017.

Mann, I. R., et al. (2008), The Upgraded CARISMA Magnetometer Array in the THEMIS era, *Space Sci. Rev.*, *141*, 413–451, doi:10.1007/s11214-008-9457-6.

Newton, R. S., D. J. Southwood, and W. J. Hughes (1978), Damping of geomagnetic pulsations by the ionosphere, *Planet. Space Sci.*, *26*, 201–209, doi:10.1016/0032-0633(78)90085-5.

Nishida, A. (1978), *Geomagnetic Diagnosis of the Magnetosphere*, 256 pp., Springer, New York.

Orr, D., and J. A. D. Matthew (1971), The variation of geomagnetic micropulsation periods with latitude and the plasmapause, *Planet. Space Sci.*, *19*, 897–905, doi:10.1016/0032-0633(71)90141-3.

Ozeke, L. G., and I. R. Mann (2001), Modeling the properties of high-m Alfvén waves driven by the drift-bounce resonance mechanism, *J. Geophys. Res.*, *106*, 15,583–15,597, doi:10.1029/2000JA000393.

Poulter, E. M., W. Allan, E. Nielsen, and K.-H. Glassmeier (1983), Stare radar observations of a Pg pulsation, *J. Geophys. Res.*, *88*, 5668–5676, doi:10.1029/JA088iA07p05668.

Poulter, E. M., W. Allan, J. G. Keys, and E. Nielsen (1984), Plasmatrough ion mass densities determined from ULF pulsation eigenperiods, *Planet. Space Sci.*, *32*, 1069–1078, doi:10.1016/0032-0633(84)90132-6.

Radoski, H. R. (1967), Highly asymmetric MHD resonances: The guided poloidal mode, *J. Geophys. Res.*, *72*, 4026–4027, doi:10.1029/JZ072i015p04026.

Rostoker, G., H. L. Lam, and J. V. Olson (1979), Pc4 giant pulsations in the morning sector, *J. Geophys. Res.*, *84*, 5153–5166, doi:10.1029/JA084iA09p05153.

Russell, C. T., P. J. Chi, D. J. Dearborn, Y. S. Ge, B. Kuo-Tiong, J. D. Means, D. R. Pierce, K. M. Rowe, and R. C. Snare (2008), THEMIS ground-based magnetometers, *Space Sci. Rev.*, *141*(1–4), 389–412, doi:10.1007/s11214-008-9337-0.

Samson, J. C., and G. Rostoker (1972), Latitude-dependent characteristics of high latitude Pc4 and Pc5 micropulsations, *J. Geophys. Res.*, *77*, 6133–6144, doi:10.1029/JA077i031p06133.

Shue, J.-H., et al. (1998), Magnetopause location under extreme solar wind conditions, *J. Geophys. Res.*, *103*, 17,691–17,700, doi:10.1029/98JA01103.

Singer, H. J., L. Matheson, R. Grubb, A. Newman, and S. D. Bouwer (1996), Monitoring space weather with the GOES magnetometers, *Proc. SPIE*, *2812*, 299, doi:10.1117/12.254077.

Southwood, D. J. (1976), A general approach to low-frequency instability in the ring current plasma, *J. Geophys. Res.*, *81*, 3340–3348, doi:10.1029/JA081i019p03340.

Southwood, D. J., and M. G. Kivelson (1997), Frequency doubling in ultra-low frequency wave signals, *J. Geophys. Res.*, *102*, 27,151–27,158, doi:10.1029/97JA02534.

Sugiura, M., and C. R. Wilson (1964), Oscillation of the geomagnetic field lines and associated magnetic perturbations at conjugate points, *J. Geophys. Res.*, *69*, 1211–1216, doi:10.1029/JZ069i007p01211.

Takahashi, K., and R. E. Denton (2007), Magnetospheric seismology using multiharmonic toroidal waves observed at geosynchronous orbit, *J. Geophys. Res.*, *112*, A05204, doi:10.1029/2006JA011709.

Takahashi, K., and R. L. McPherron (1982), Harmonic structure of Pc3–4 pulsations, *J. Geophys. Res.*, *87*, 1504–1516, doi:10.1029/JA087iA03p01504.

Takahashi, K., and R. L. McPherron (1984), Standing hydromagnetic oscillations in the magnetosphere, *Planet. Space Sci.*, *32*, 1343–1359, doi:10.1016/0032-0633(84)90078-3.

Takahashi, K., J. F. Fennell, E. Amata, and P. R. Higbie (1987), Field-aligned structure of the storm time Pc5 wave of November 14–15, 1979, *J. Geophys. Res.*, *92*, 5857–5864, doi:10.1029/JA092iA06p05857.

Takahashi, K., N. Sato, J. Warnecke, H. Lühr, H. E. Spence, and Y. Tonegawa (1992), On the standing wave mode of giant pulsations, *J. Geophys. Res.*, *97*, 10,717–10,732, doi:10.1029/92JA00382.

Takahashi, K., B. J. Anderson, and S. Ohtani (1996), Multisatellite study of nightside transient toroidal waves, *J. Geophys. Res.*, *101*, 24,815–24,825, doi:10.1029/96JA02045.

Takahashi, K., R. E. Denton, R. R. Anderson, and W. J. Hughes (2006), Mass density inferred from toroidal wave frequencies and its comparison to electron density, *J. Geophys. Res.*, *111*, A01201, doi:10.1029/2005JA011286.

Takahashi, K., R. E. Denton, and H. J. Singer (2010), Solar cycle variation of geosynchronous plasma mass density derived from the frequency of standing Alfvén waves, *J. Geophys. Res.*, *115*, A07207, doi:10.1029/2009JA015243.

Thompson, S. M., and M. G. Kivelson (2001), New evidence for the origin of giant pulsations, *J. Geophys. Res.*, *106*, 21,237–21,253, doi:10.1029/2001JA000026.

Tonegawa, Y., and N. Sato (1987), Conjugate area study of giant geomagnetic pulsations, paper presented at Chapman Conference on Plasma Waves and Instabilities in Magnetospheres and at Comets, Sohbun, Sendai/Mt. Zao, Japan, 12–16 October.

Troitskaya, V. A., T. A. Plyasova-Bakounina, and A. V. Gul'yel'mi (1971), Relationship between Pc2–4 pulsations and the interplanetary magnetic field, *Dokl. Akad. Nauk SSSR*, *197*, 1312–1314.

Tsyganenko, N. A. (1989), A magnetospheric magnetic field model with a warped tail current sheet, *Planet. Space Sci.*, *37*, 5–20, doi:10.1016/0032-0633(89)90066-4.

Veldkamp, J. (1960), A giant geomagnetic pulsation, *J. Atmos. Terr. Phys.*, *17*, 320–324, doi:10.1016/0021-9169(60)90146-X.

Westphal, K. O., and J. A. Jacobs (1962), Oscillations of the earth's outer magnetosphere and micropulsations, *J. Roy. Astron. Soc.*, *6*, 360–376.

Wilson, M. E., T. K. Yeoman, L. J. Baddeley, and B. J. Kellet (2006), A Statistical investigation of the invariant latitude dependence of unstable magnetospheric ion populations in relation to high m ULF wave generation, *Ann. Geophys.*, *24*, 3027–3040, doi:10.5194/angeo-24-3027-2006.

Wright, D. M., T. K. Yeoman, I. J. Rae, J. Storey, A. B. Stockton-Chalk, J. L. Roeder, and K. J. Trattner (2001), Ground-based and Polar spacecraft observations of a giant (Pg) pulsation and its associated source mechanism, *J. Geophys. Res.*, *106*, 10,837–10,852, doi:10.1029/2001JA900022.

Yeoman, T. K., and D. M. Wright (2001), ULF waves with drift resonance and drift-bounce resonance energy sources as observed in artificially induced HF radar backscatter, *Ann. Geophys.*, *19*, 159–170, doi:10.5194/angeo-19-159-2001.

Yeoman, T. K., D. M. Wright, P. J. Chapman, and A. B. Stockton-Chalk (2000), High-latitude observations of ULF waves with large azimuthal wavenumbers, *J. Geophys. Res.*, *105*, 5453–5462, doi:10.1029/1999JA005081.

Yeoman, T. K., D. M. Wright, and L. J. Baddeley (2006), Ionospheric signatures of ULF waves: Active radar techniques, in *Magnetospheric ULF Waves: Synthesis and New Directions*, *169*, edited by K. Takahashi, P. J. Chi, R. E. Denton, and R. L. Lysak, 359 pp., AGU, Washington, DC.

V. Angelopoulos and C. T. Russell, Institute of Geophysics and Planetary Physics and Department of Earth and Space Sciences, University of California, 3845 Slichter Hall, 603 Charles Young Dr. E., Los Angeles, CA 90095-1567, USA.

J. Bonnell, Space Sciences Laboratory, University of California, Berkeley, CA 94720-7450, USA.

K.-H. Glassmeier, Institute for Geophysics and Extraterrestrial Physics, Technical University of Braunschweig, Mendelssohnstr. 3, Braunschweig D-38106, Germany.

Y. Nishimura, Department of Atmospheric and Oceanic Sciences, University of California, 405 Hilgard Ave., Los Angeles, CA 90095-1565, USA.

H. J. Singer, NOAA Space Weather Prediction Center, 325 Broadway, Boulder, CO 80305, USA.

K. Takahashi, The Johns Hopkins University Applied Physics Laboratory, Laurel, MD 20723-6099, USA. (kazue.takahashi@jhuapl.edu)